



## Global-global interaction in cold-formed steel channel columns: Relevance, post-buckling behavior, strength and DSM design

Pedro B. Dinis<sup>1</sup>, Dinar Camotim<sup>1</sup>, André D. Martins<sup>1</sup>, Alexandre Landesmann<sup>2</sup>

### Abstract

In the context of investigations on the accuracy of the current Direct Strength Method (DSM) column global design curve in predicting cold-formed steel column major-axis flexural-torsional failures, the authors unveiled that, depending on the column length and end support conditions, its failure load may be eroded by the interaction between the first two global buckling modes: a major-axis flexural-torsional ( $F_{MT}$  – critical) one and a minor-axis flexural ( $F_m$ ) one – a global-global (G-G) interaction. This finding provided the root and motivation for the research effort whose first fruits are reported in this paper, which presents and discusses the results of an ongoing numerical investigation on the behavior and DSM design of cold-formed steel columns buckling in  $F_{MT}$  modes and experiencing G-G interaction – only fixed-ended plain channel columns are dealt with. After reviewing the DSM-based design approach proposed by Dinis *et al.* (2020) to predict column  $F_{MT}$  failures, the paper addresses the column (i) buckling behavior, crucial to select columns prone to G-G interaction, and (ii)  $F_{MT}$  post-buckling behavior – particular attention paid to identifying the most detrimental initial geometrical imperfection. Then, after obtaining the selected column  $F_{MT}$  failure loads for five yield stresses (wide slenderness range covered), these failure loads are used (i) to show the inadequacy of the existing DSM-based design approach in predicting them and (ii) as the basis for its modification, which involves the  $F_{MT}$ -to- $F_m$  buckling load ratio and makes it possible to handle adequately also G-G interactive failures. The quality of the findings reported provides strong encouragement to proceed along this path, as the methodology adopted is expected to succeed also for columns with other cross-section shapes and/or end support conditions.

### 1. Introduction and Motivation

Cold-formed steel members invariably display very slender thin-walled open cross-sections, a feature making them highly susceptible to several instability phenomena, namely local, distortional and global (flexural or flexural-torsional) buckling – Figs. 1(a)-(c), concerning channel columns, show buckled cross-sections associated with local, flexural-torsional and flexural buckling. Therefore, their overall structural response and ultimate strength are affected, to a larger or smaller extent, by such instability phenomena – this explains why they must be incorporated in cold-formed steel specifications (they can only be ignored in the design of stocky members, exhibiting “compact” cross-sections).

---

<sup>1</sup> CERIS, ICIST, DECivil, Instituto Superior Técnico, Universidade de Lisboa, Portugal. <dinis@civil.ist.utl.pt; dcamotim@civil.ist.utl.pt; andrerdmartins@ist.utl.pt>

<sup>2</sup> Civil Engineering Program, COPPE, Universidade Federal do Rio de Janeiro, Brazil. <alandes@coc.ufrj.br>

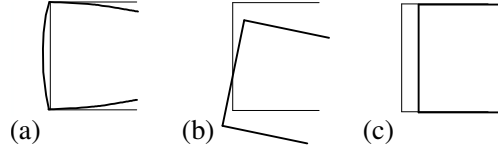


**Figure 1:** Channel column buckled cross-sections concerning (a) local, (b) flexural-torsional and (c) flexural modes

Nowadays, it can be rightfully argued that the Direct Strength Method (DSM – *e.g.*, Schafer 2008, 2019 or Camotim *et al.* 2016), first proposed by Schafer & Peköz (1998) and based on an original idea of Hancock *et al.* (1994), is the most rational and efficient approach for the design of cold-formed steel members (columns and beams, to be more precise) – this explains its fast growing and widespread popularity around the world. Moreover, it should be noted that the domain of application of the DSM has been recently extended to cover also beam-columns (Torabian & Schafer 2018), even if this research effort did not yet reach the codification stage. The currently codified design/strength curves are able to handle local, distortional, global and local-global interactive failures. In the context of this investigation, the relevant nominal strength is the global one ( $P_{nG}$ ), which is given by

$$P_{nG} = \begin{cases} P_y \left( 0.658^{\lambda_G^2} \right) & \text{if } \lambda_G \leq 1.5 \\ P_y \left( \frac{0.877}{\lambda_G^2} \right) & \text{if } \lambda_G > 1.5 \end{cases} \quad \text{with} \quad \lambda_G = \sqrt{\frac{P_y}{P_{crG}}} \quad , \quad (1)$$

where  $P_{crG}$  and  $\lambda_G$  are the column global critical buckling load and slenderness, and  $P_y = Af_y$  is the column squash load ( $A$  and  $f_y$  are the cross-sectional area and steel yield stress, respectively). This design curve, combining an exponential expression (Ziemian 2010) with the (lowered) Euler curve, was first included in the North American cold-formed steel design specification in 1996 (AISI 1996), due to the work of Peköz & Sümer (1992), who showed that the above design curve, previously codified in the context of hot-rolled steel members used in buildings (AISC 1986), yielded a better failure load prediction quality than that adopted at that time by the cold-formed steel community (AISI 1986).

Recently, the authors (Dinis *et al.* 2019, 2020) reported numerical investigations intended to assess the accuracy of the current DSM column global strength curve in predicting the failure loads of fixed-ended cold-formed steel columns collapsing in major-axis flexural-torsional ( $F_{MT}$ ) or minor-axis flexural ( $F_m$ ) modes – an extensive parametric study was carried out in order to gather failure loads of columns (i) exhibiting a wide variety of cross-section shapes (plain channels, unstiffened, return lip, web-stiffened and web/flange-stiffened lipped channels, lipped zed-sections, hat-sections, rack-sections and I-sections formed by back-to-back plain channels), (ii) various geometries (cross-section dimensions and lengths) and (iii) covering a wide slenderness range. While the failure loads of columns collapsing in  $F_m$  modes were found to be quite well predicted (there is only room for slight improvements in the low and intermediate slenderness ranges), it was shown that those associated with  $F_{MT}$  failure modes are often considerably underestimated by the current design curve in the moderate and high slenderness ranges. This fact led the authors (Dinis *et al.* 2020) to propose a novel DSM-based set of strength curves ( $P_{nFT}$ ), dependent on a non-dimensional cross-section geometric parameter involving the area, major and minor moments of inertia, and warping constant<sup>3</sup>. This strength curve set was shown to lead to safe and accurate

<sup>3</sup> In order to make a clear distinction between the current DSM global design curve and the proposed DSM-based strength curve set, concerning exclusively columns failing in  $F_{MT}$  modes, the subscript “G” was replaced by “FT” in the latter.

fixed-ended column  $F_{MT}$  failure load predictions, which eliminate the large underestimations and scatter associated with the codified  $P_{nG}$  curve when the slenderness is moderate or high (above 1.5).

Dinis *et al.* (2020) also investigated cold-formed steel columns failing in  $F_{MT}$  modes and exhibiting other than fixed-ended support conditions (F columns), namely three types of pinned supports, all of them fixed with respect to torsion and having warping fully prevented: supports consisting of hinges that are either cylindrical (pinned with respect to major *or* minor-axis bending –  $PC_M$  and  $PC_m$  columns) or spherical (pinned with respect to major *and* minor-axis bending – PS columns) – the investigation involved trios of identical  $PC_M$ ,  $PC_m$  and PS columns with plain channel, lipped channel, return lipped channel, hat and rack cross-sections. In this context, it was unveiled that the currently codified DSM column global design curve ( $P_{nG}$ ) (i) predicts adequately (safely and accurately) the  $F_{MT}$  failure loads of the PS columns, along the whole slenderness range, (ii) underestimates the  $F_{MT}$  failure loads of the  $PC_M$  columns with  $\lambda_{FT} > 1.5$  (but by smaller amounts than their F counterparts) and (iii) overestimates the  $F_{MT}$  failure loads of the  $PC_m$  columns with  $\lambda_{FT} > 1.0$ . In other words, it was concluded that the  $F_{MT}$  failure load prediction quality provided by the  $P_{nG}$  values varies considerably with the column end support conditions – this unexpected conclusion led the authors to further investigate this issue.

A close inspection of the columns analyzed revealed that there is a major difference between the F+ $PC_M$  and  $PC_m$ +PS column pairs, concerning the closeness between the  $F_{MT}$  (critical –  $P_{cr,FT}$ ) and  $F_m$  (non-critical –  $P_{b,fm}$ ) buckling loads, *i.e.*, the closeness of the ratio  $P_{b,fm}/P_{cr,FT}$  to 1.0: much closer in the latter than in the former. Moreover, it was also found that it is virtually impossible to select  $PC_m$  or PS column geometries that preclude the closeness between the two buckling loads ( $P_{b,fm}/P_{cr,FT}$  is always fairly close to 1.0) – unlike in F or  $PC_M$  columns, for which an appropriate geometry selection enables a fine “control” of the closeness between them ( $P_{b,fm}/P_{cr,FT}$  can be either much higher, moderately higher or close to 1.0). This finding raised the suspicion (initially) and convinced the authors (subsequently) that the column  $F_{MT}$  post-buckling behavior and strength is bound to be influenced by the coupling between  $F_{MT}$  and  $F_m$  buckling – the closeness of  $P_{b,fm}/P_{cr,FT}$  to 1.0 indicates how relevant is this interaction phenomenon. At this stage, it is worth mentioning that, to the authors’ best knowledge, such a global-global coupling phenomenon has only been investigated in the context of short-to-intermediate equal-leg angle columns (*e.g.*, Dinis *et al.* 2012, Dinis & Camotim 2015, Camotim *et al.* 2019), which exhibit a very peculiar structural behavior stemming from their geometrical simplicity: that they are formed by just two outstand walls and, therefore, exhibit very similar flexural-torsional and local deformations. Conversely, the global-global interaction addressed in this work is bound to occur in columns with singly symmetric cross-sections (symmetry with respect to the major-axis) and  $F_{MT}$  critical buckling modes.

In view of the content of the previous paragraph, it can be logically argued that (i) the  $PC_m$  and PS columns are invariably affected by  $F_{MT}$ - $F_m$  (global-global) interaction, while (ii) the F and  $PC_M$  columns may be affected by this coupling phenomenon or not, depending on the closeness of  $P_{b,FM}/P_{cr,FT}$  to 1.0. Therefore, in order to assess the relevance of global-global interaction in eroding the column  $F_{MT}$  failure loads, it was decided to compare the failure loads of two sets of cold-formed steel fixed-ended plain channel (U) columns sharing the same cross-section dimensions ( $b_w=100$  mm,  $b_f=40$  mm,  $t=1.2$  mm.), yield stresses and initial geometrical imperfections (critical-mode  $F_{MT}$  imperfections with amplitude  $L/1000$ ). The two sets only differ in the column lengths, selected to ensure  $P_{b,FM}/P_{cr,FT}$  values that are either much higher than 1.0 (first set) or fairly close to 1.0 (second set) – all the columns in both sets have critical  $F_{MT}$  buckling modes. Moreover, only columns with slenderness values higher than about 1.5 were considered, since the interaction effects are always stronger in slender columns. Fig. 2 displays the plots  $P_u/P_{nFT}$  vs  $\lambda_{FT}$  for the two sets of fixed-ended U columns – the white and grey circles stand, respectively, for the columns with

$P_{b,FM}/P_{b,FT}$  values quite higher than 1.0 ( $P_{b,FM}/P_{cr,FT} \geq 1.45$ ) and very close to 1.0 ( $P_{b,FM}/P_{cr,FT} < 1.35$ ). It is clear that, as expected, the white  $P_u/P_{b,FT}$  values are consistently well above their grey counterparts, evidencing the failure load erosion caused by the global-global interaction. In addition, it is also observed that the  $P_{nFT}$  estimation of the second (grey) failure load set is clearly inadequate (inaccurate and unsafe) – indeed, almost all  $P_u/P_{nFT}$  values are below 1.0 (a large fraction of them substantially). Conversely, the same estimation of the first (white) failure load set is very good – not surprising, since the development and validation of the  $P_{nFT}$  DSM-based design approach was based, almost solely, on failure loads of columns with  $P_{b,FM}/P_{cr,FT}$  values much higher than 1.0 (Dinis *et al.* 2020). The corresponding statistical indicators (mean, standard deviation and maximum/minimum values) make it possible to quantify the difference in failure load prediction quality: they read 0.74-0.14-1.01-0.50 (grey circles) vs. 1.08-0.08-1.21-0.85 (white circles) and show the inadequacy of the  $P_{nFT}$  values in predicting failure loads of columns affected by global-global interaction. This finding provided the motivation for the research effort whose first results are reported in this work.

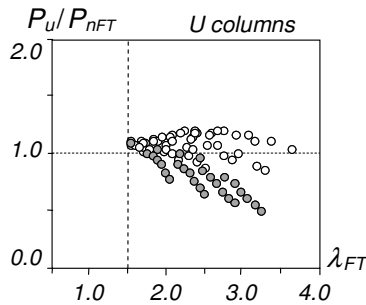


**Figure 2:** Plots  $P_u/P_{nFT}$  vs.  $\lambda_{FT}$  for F U columns with  $P_{b,FM}/P_{b,FT}$  values higher than (white circles) and close to (grey circles) 1.0

The aim of this work is to present and discuss the available results of an ongoing numerical investigation on the post-buckling behavior, strength and DSM design of cold-formed steel columns buckling in  $F_{MT}$  modes and experiencing global-global (G-G) interaction – this paper deals exclusively with fixed-ended plain channel (U) columns. After presenting an overview of the main features and merits of the DSM-based strength curve set ( $P_{nFT}$ ) recently proposed by Dinis *et al.* (2020) to predict column flexural-torsional ( $F_{MT}$ ) failure loads, the paper addresses the column buckling behavior and the selection of column geometries prone to various levels of G-G interaction. Then, the elastic and elastic-plastic post-buckling behavior and strength of fixed-ended U columns affected by G-G interaction is investigated – particular attention is paid to the identification of the most detrimental critical-mode initial geometrical imperfection shape, in the sense that it leads to the lowest column  $F_{MT}$  strengths and failure loads. Next, the paper presents the results of a parametric study carried out to gather  $F_{MT}$  failure loads of U columns with (i) the various geometries selected earlier and (ii) several yield stresses, chosen to enable covering a wide slenderness range. Then, the assembled numerical  $F_{MT}$  failure load data are used (i) to show that the DSM-based strength curve set proposed by Dinis *et al.* (2020) is unable to adequately predict them and (ii) as the basis to search for an improved DSM-based design approach able to handle also G-G interactive failures of columns buckling in  $F_{MT}$  modes. It is shown that this search was successful and leads to a modification of the column strength curve set proposed by Dinis *et al.* (2020) – it involves incorporating the buckling load ratio  $R_G = P_{b,FM}/P_{cr,FT}$  in the expressions providing the strength curves, thus accounting for the level of G-G interaction. The modified DSM-based design approach predicts quite adequately (safely and accurately) the failure loads of fixed-ended U columns buckling in  $F_{MT}$  modes and affected by G-G interaction, and, at the same time, retains the high failure load prediction quality for the columns

unaffected by this interaction. Although this work is restricted to fixed-ended U columns, the quality of the findings reported provides strong encouragement to proceed along this path, as the methodology adopted is expected to succeed also for columns with other cross-section shapes and/or end support conditions.

## 2. Overview of the Novel DSM-Based Design Approach for Columns Failing in F<sub>M</sub>T Modes

The authors (Dinis *et al.* 2020) have recently developed and validated a DSM-based design approach intended to predict adequately (safely and accurately) the fixed-ended (F) column F<sub>M</sub>T failure loads – they showed that the currently codified DSM column global design curve often underestimates quite substantially the F<sub>M</sub>T failure loads of columns with slenderness higher than 1.5. On the basis of a rather extensive set of numerical F<sub>M</sub>T failure loads, concerning columns with several cross-section shapes (plain channels, hat-section, rack-sections and unstiffened, return lip, web-stiffened and web/flange-stiffened lipped channels) and dimensions, lengths and yield stresses, the authors showed that no single strength curve is able to predict adequately all the numerical F<sub>M</sub>T failure load assembled. Instead, they concluded that it is indispensable to have a strength curve set. After a considerable research effort, they found that it is necessary (i) to group the columns according to the value of a cross-section geometric parameter, termed  $\beta_{FT}$  and defines as

$$\beta_{FT} = \frac{I_I + I_w/A}{I_{II}} \quad , \quad (2)$$

and (ii) to have a different strength curve for the columns sharing the same  $\beta_{FT}$  value. In Eq. (2),  $A$ ,  $I_I$ ,  $I_{II}$  and  $I_w$  are the cross-section area, major and minor moments of inertia, and warping constant – note that, nowadays,  $I_w$  can be easily calculated numerically, by means of freely available codes such as CUFISM (Li *et al.* 2014) or GBTUL (Bebiano *et al.* 2018). The subsequent calibration of the sought DSM-based  $\beta_{FT}$ -dependent strength curve set led to

$$P_{nFT} = \begin{cases} P_y \left( 0.658 \lambda_{FT}^2 \right) & \text{if } \lambda_{FT} \leq 1.5 \\ P_y \left( \frac{a}{\lambda_{FT}^b} \right) & \text{if } \lambda_{FT} > 1.5 \end{cases} \quad \text{with} \quad \lambda_{FT} = \sqrt{\frac{P_y}{P_{crFT}}} \quad , \quad (3)$$

where the  $\beta_{FT}$ -dependence is felt through parameters  $a$  and  $b$ , obtained by means of a “trial-and-error curve fitting procedure”, which read

$$a = 0.39 \times 1.5^b \quad b = 0.06 \beta_{FT} + 0.71 \leq 2.0 \quad . \quad (4)$$

It should be noted that the strength curve set defined by Eq. (3) only differs from the current DSM column global design curve for  $\lambda_{FT} > 1.5$  (moderate and high slenderness ranges) – the exponential expression is kept in the low-to-moderate slenderness range ( $\lambda_{FT} \leq 1.5$ ). Each  $\beta_{FT}$  value leads to  $a$  and  $b$  values defining a different strength curve. For  $\beta_{FT} \geq 21.5$ , one has  $b=2.0$  and  $a=0.877$ , which means that Eq. (3) coincides with Eq. (1) (current DSM column global design strength curve).

Figs. 3(a)-(b) plot, against  $\lambda_{FT}$  ( $=\lambda_G$ ), the  $P_u/P_{nG}$  and  $P_u/P_{nFT}$  values concerning all numerical failure loads considered by Dinis *et al.* (2020) – recall that the two plots only differ for  $\lambda_{FT} > 1.5$ . Both figures include the  $P_u/P_{nG}$  and  $P_u/P_{nFT}$  means, standard deviations and maximum/minimum values, as well as the

LRFD resistance factor  $\phi$  values (AISI 2016) they lead to. It is clear that the proposed strength curve set yields accurate and mostly safe  $F_{MT}$  failure load predictions: the  $P_u/P_{nFT}$  mean and standard deviation are equal to 1.061-0.054 and lead to a LRFD resistance factor much higher than that prescribed by AISI (2016) for compression members ( $\phi_c=0.85$ ).

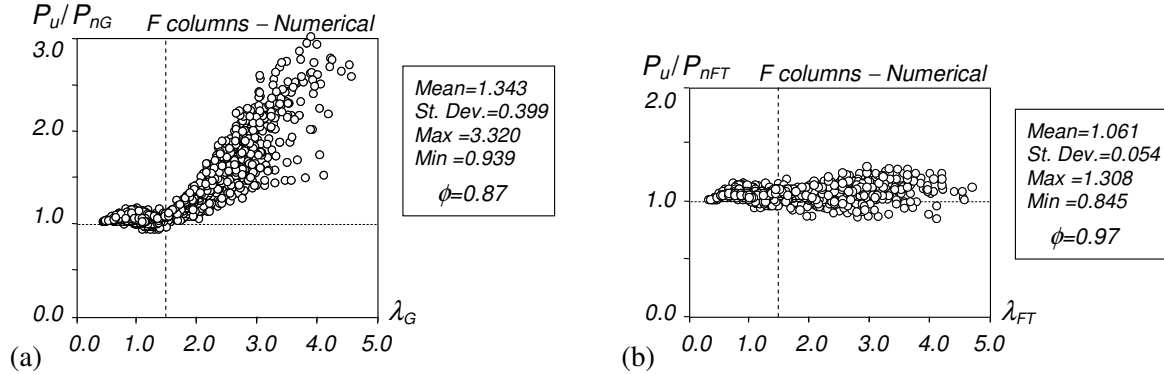


Figure 3: Plots (a)  $P_u/P_{nG}$  vs.  $\lambda_G$  and (b)  $P_u/P_{nFT}$  vs.  $\lambda_{FT}$  for the numerical  $F_{MT}$  failure loads considered by Dinis *et al.* (2020)

### 3. Column Geometry Selection – Buckling Behavior

The signature curves depicted in Fig. 4(a) concern steel ( $E=210\text{GPa}$ ,  $\nu=0.3$ ) U columns with  $b_w=100\text{mm}$ ,  $b_f=80\text{mm}$  and four thickness values, namely  $t=2;3;4;5\text{mm}$ . Each solid curve provides the variation, with the length  $L$  (logarithmic scale), of the critical buckling stress  $f_{cr}$  and was obtained by means of GBT buckling analyses performed in the code GBTUL (Bebiano *et al.* 2018) and including 9 deformation modes: 4 global (1-4) and 5 local (5-9). The dashed curve provides the variation of the minor-axis flexural

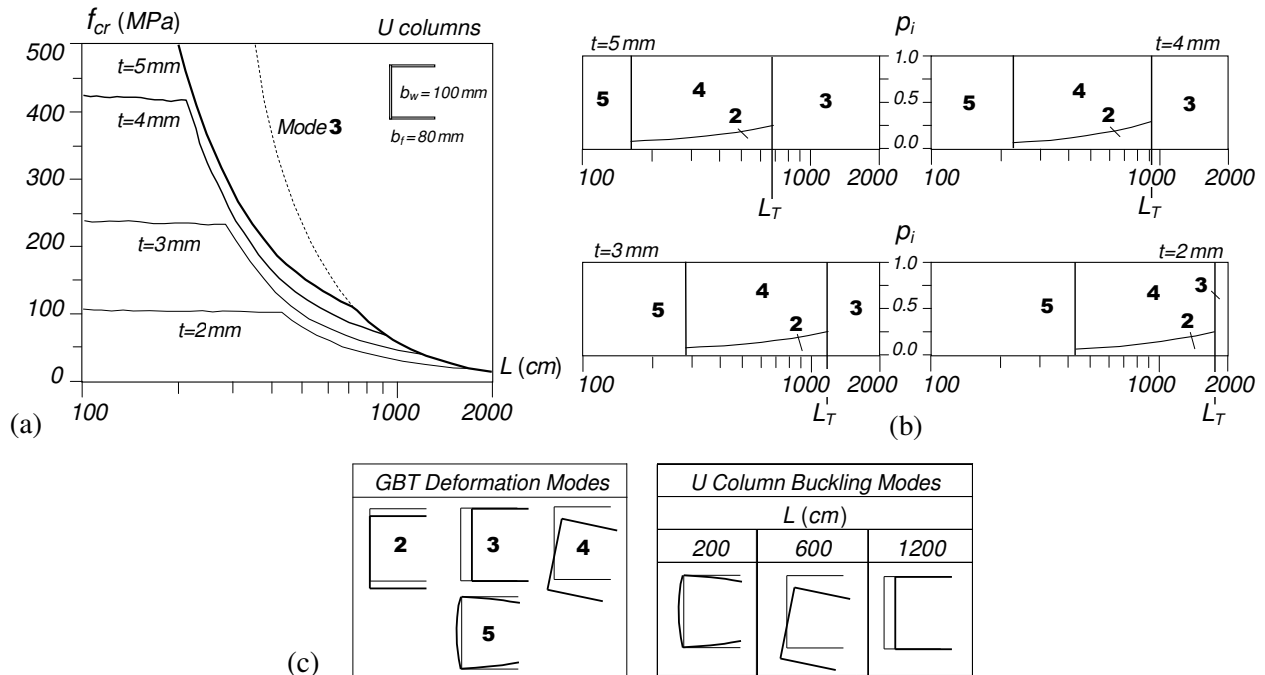


Figure 4: (a)  $f_{cr}$  vs.  $L$  curves and (b) GBT modal participation diagrams of U columns ( $b_w=100\text{mm}$ ;  $b_f=80\text{mm}$ ;  $t=2;3;4;5\text{mm}$ ), and (c) in-plane shapes of GBT deformation modes 2-5 and three critical buckling modes of  $t=3\text{mm}$  U columns

buckling stress  $f_{b.Fm}$  with  $L$  – this curve is the same for the 4 cross-section geometries. Figs. 4(b) show the GBT modal participation diagrams associated with each  $f_{cr}$  vs.  $L$  curve, providing the contributions of each GBT deformation mode to the column buckling modes (e.g., a  $t=3$  mm column with  $L=500$  cm buckles in a mode combining participations from modes **2, 4** – 10.5% and 89.5%, respectively). Finally, Fig. 4(c) shows the in-plane shapes of the GBT deformation modes **2-5** and the critical buckling modes of  $t=3$  mm U columns with  $L=200, 600, 1200$  cm. These buckling results prompt the following remarks:

- (i) Each  $f_{cr}$  vs.  $L$  curve exhibits two distinct zones, one associated with local buckling in modes with several half-waves (only  $p_5$  exists and  $f_{cr}$  remains constant) and the other with single half-wave global buckling. In the latter zone,  $f_{cr}$  decreases monotonically with  $L$  and the columns buckle in either  $F_{MT}$  (**2+4**) modes with dominant torsional deformation or in  $F_m$  (**3**) modes – the change in buckling mode nature occurs abruptly, at the “transition length”  $L=L_T$ .
- (ii) Since the column  $F_m$  buckling stress is independent of  $t$ , the 4  $F_{MT}$  signature curve branches, which concern columns with different  $t$  values, end in a common  $F_m$  signature curve branch – see Fig. 4(a).
- (iii) Columns with  $L=L_T$  have coincident  $F_{MT}$  and  $F_m$  buckling stresses, which means that their post-buckling behaviors, strengths and failure loads are bound to be affected by the interaction between these two buckling modes (G-G interaction). However, it is expected that the interaction effects will also influence the post-buckling behavior, strength and failure load of columns with lengths not too much smaller than  $L_T$ , i.e., such that the ratio  $f_{b.Fm}/f_{cr} (\equiv P_{b.Fm}/P_{cr.FT})$  is not significantly higher than 1.0.

It is now necessary to identify column geometries associated with several levels of closeness between the column  $f_{cr}$  and  $f_{b.Fm}$  buckling stresses. This is done by selecting columns with lengths lower than  $L_T$  (see Fig. 4(b)) – a limit  $L=950$  cm was defined to ensure that the columns selected are not unrealistically long. The 47 column geometries ( $b_w, b_f, t, L$ ) selected to ensure buckling in  $F_{MT}$  and  $f_{b.Fm}/f_{cr}$  ratios comprised between 1.87 and 1.0. Table 1 provided the selected column cross-section dimensions and properties ( $b_w, b_f, t, A, b_w/b_f, I_t, I_{II}, I_w$  and  $\beta_{FT}$ ), lengths ( $L_i$ ) and buckling stresses and ratios ( $f_{cr}, f_{b.Fm}$  and  $f_{b.Fm}/f_{cr} \equiv R_G$ ). It is worth noting that (i) there are 8 cross-section geometries whose dimensions such that  $2.50 \geq b_w/b_f \geq 1.00$  and  $18.13 \geq \beta_{FT} \geq 2.65$ , and (ii) the lengths are such that  $9500 \geq L \geq 2200$  mm – 7 out of the 8 cross-section geometries selected are combined with several (6 or 7) lengths, thus enabling a variation of the  $R_G$  value.

#### 4. Post-Buckling Behavior under Global-Global Mode Interaction – Imperfection-Sensitivity Study

A very important issue in mode interaction studies is to assess how the initial geometrical imperfection shape influences the post-buckling behavior and strength of the structural system under scrutiny – i.e., to perform an imperfection-sensitivity study. In particular, it is essential to identify the most detrimental initial imperfection shape, in the sense that it leads to the lowest strengths. In this particular case, the aim is to find the initial imperfection shape, combining arbitrarily  $F_{MT}$  and  $F_m$  components, that leads to the lowest column  $F_{MT}$  strengths and failure loads. The elastic and elastic-plastic results presented were obtained by means of ABAQUS non-linear shell finite element analyses SFEA, using a model identical to that previously employed by Dinis *et al.* (2019, 2020) – rounded corner and residual stress effects were disregarded, since they are known to practically cancel each other (e.g., Ellobody & Young 2005).

##### 4.1 Elastic Post-Buckling Strength – Most Detrimental Initial Geometrical Imperfections

Due to the presence of two competing buckling modes in columns affected by global-global interaction (critical  $F_{MT}$  and non-critical  $F_m$  modes), the commonly used approach of considering critical-mode initial imperfections ceases to be adequate. Indeed, in order to identify the most detrimental initial imperfection shape, it is necessary to determine and compare equilibrium paths of otherwise identical columns with

**Table 1:** Selected U column geometries:  $b_w$ ,  $b_f$ ,  $t$ ,  $A$ ,  $I_I$ ,  $I_{II}$ ,  $I_w$ ,  $L$ ,  $f_{cr}$  and  $f_{b,FM}$  values (mm, mm<sup>2</sup>, mm<sup>4</sup>, mm<sup>6</sup> and MPa)

Column	$b_w$	$b_f$	$t$	$A$ ( $\times 10^2$ )	$b_w/b_f$	$I_I$ ( $\times 10^4$ )	$I_{II}$ ( $\times 10^4$ )	$I_w$ ( $\times 10^6$ )	$\beta_{FT}$	$L$		$f_{cr}$	$f_{b,FM}$	$R_G$
U1	100	40	1.2	2.16	2.50	34.0	3.4	60.3	18.13	$L_1$	3700	89.7	95.4	1.06
										$L_2$	3800	85.9	90.5	1.05
										$L_3$	3900	82.4	86.0	1.04
										$L_4$	4000	79.1	81.7	1.03
										$L_5$	4100	76.0	77.8	1.02
										$L_6$	4200	73.3	74.2	1.01
										$L_7$	4300	70.6	70.8	1.00
U2	100	40	2.0	3.6	2.50	56.7	5.7	100.5	14.85	$L_1$	2200	252.9	268.4	1.06
U3	100	60	2.0	4.4	1.67	76.7	17.0	297.7	8.48	$L_1$	4000	115.9	200.5	1.73
										$L_2$	4500	97.0	158.3	1.63
										$L_3$	6000	65.5	89.1	1.36
										$L_4$	7000	54.5	65.5	1.20
										$L_5$	7500	50.5	57.0	1.13
										$L_6$	8000	47.2	50.1	1.06
U4	100	60	3.0	6.6	1.67	115.0	25.5	447.1	7.15	$L_1$	3300	190.3	294.4	1.55
										$L_2$	3700	163.0	234.3	1.44
										$L_3$	4100	143.0	190.9	1.33
										$L_4$	4600	124.8	151.7	1.22
										$L_5$	5000	113.8	128.4	1.13
										$L_6$	5300	107.0	114.3	1.07
										$L_7$	5600	101.3	102.3	1.01
U5	100	80	4.0	10.4	1.25	193.4	73.6	1300.2	4.33	$L_1$	5000	125.4	234.6	1.87
										$L_2$	6500	96.5	138.8	1.44
										$L_3$	7000	89.1	119.7	1.34
										$L_4$	7500	83.6	104.3	1.25
										$L_5$	8000	78.9	91.7	1.16
										$L_6$	8500	74.7	81.2	1.09
										$L_7$	9000	71.0	72.4	1.02
U6	100	80	5.0	13.0	1.25	241.8	92.0	1629.1	3.99	$L_1$	4900	158.5	244.4	1.54
										$L_2$	5300	146.8	208.9	1.42
										$L_3$	5700	137.1	180.6	1.32
										$L_4$	6100	128.9	157.7	1.22
										$L_5$	6600	120.0	134.7	1.12
										$L_6$	6900	115.3	123.3	1.07
										$L_7$	7300	109.6	110.1	1.01
U7	80	80	5.0	12.0	1.00	149.5	85.4	985.8	2.71	$L_1$	6500	100.7	139.7	1.39
										$L_2$	7000	94.0	120.5	1.28
										$L_3$	7500	87.8	104.9	1.19
										$L_4$	8000	82.1	92.2	1.12
										$L_5$	8500	76.9	81.7	1.06
										$L_6$	9000	72.2	72.9	1.01
U8	90	90	6.0	16.2	1.00	255.5	146.0	2134.8	2.65	$L_1$	7000	112.7	152.5	1.35
										$L_2$	7500	105.4	132.8	1.26
										$L_3$	8000	98.8	116.7	1.18
										$L_4$	8500	92.7	103.4	1.12
										$L_5$	9000	87.2	92.2	1.06
										$L_6$	9500	82.1	82.8	1.01

initial geometrical imperfections that (i) span the whole critical-mode shape range and (ii) share a common amplitude. A systematic approach to identify the most detrimental initial geometrical imperfection shape was devised by Camotim & Dinis (2011) and accounts for the fact that the two competing buckling modes exhibit a single half-wave – it involves the performance of the following procedures:

- (i) Determine “pure” critical buckling mode shapes, normalized to exhibit unit mid-span displacements: (i<sub>1</sub>) a F<sub>M</sub>T mode with a flange-lip corner downward vertical displacement equal to  $v_{FT}=1$  mm and (i<sub>2</sub>) two F<sub>m</sub> modes with uniform horizontal displacements equal to  $w_{Fm}=1$  mm (moving to the right) and  $w_{Fm}=-1$  mm (moving to the left) – the need to consider the two F<sub>m</sub> modes stems from the fact that they correspond to different post-buckling behaviors, as will be shown a bit ahead in the paper.
- (ii) To scale the three “pure” modes, so that their amplitudes equal  $L/1000$  (value commonly prescribed in cold-formed steel specifications).
- (iii) A given initial geometrical imperfection shape is obtained by linearly combining the scaled buckling modes shapes, with coefficients  $C_{FT,0}$  and  $C_{Fm,0}$  satisfying the condition  $(C_{FT,0})^2+(C_{Fm,0})^2=1$ . A better visualization and “feel” of the initial imperfection shapes considered can be obtained by considering the unit radius half circle drawn on the  $C_{FT,0}$ - $C_{Fm,0}$  plane, as shown in Fig. 5(a)<sup>4</sup>. Each possible critical-mode imperfection shape corresponds to a point lying on this half circle, associated with an angle  $\theta$ , measured from the horizontal ( $C_{FT,0}$ ) axis and positive when counterclockwise – it defines a  $C_{Fm,0}/C_{FT,0}$  ratio, where  $C_{FT,0}=\cos\theta$  and  $C_{Fm,0}=\sin\theta$ . Fig. 5(b) shows the pure FT and F<sub>m</sub> initial imperfection shapes ( $\theta=0^\circ$ ;  $\theta=90^\circ$ ;  $\theta=-90^\circ$ ).

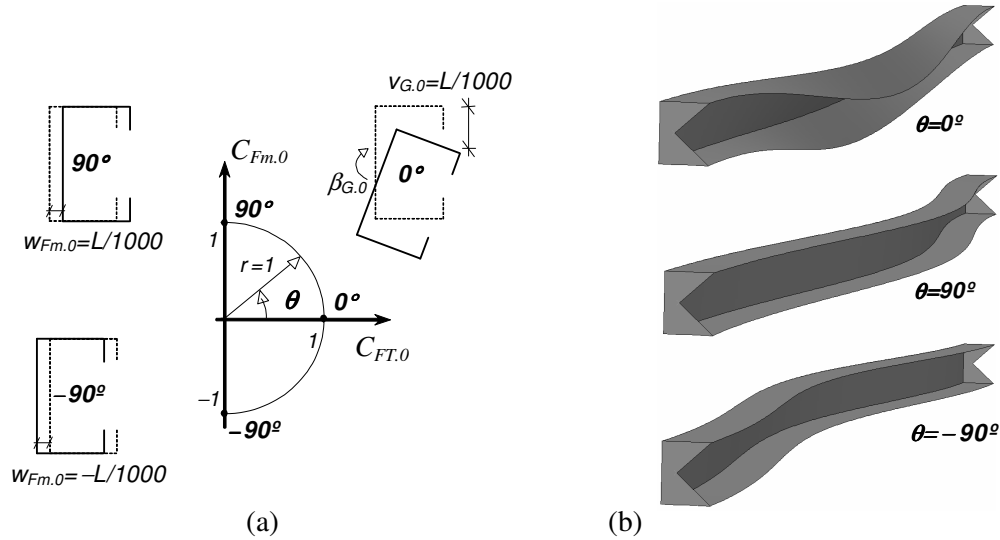


**Figure 5.** (a) Initial imperfection representation in the  $C_{FT,0}$ - $C_{Fm,0}$  plane and (b) initial imperfection shapes for  $\theta=0^\circ, \pm 90^\circ$

After having defined the full set of possible critical-mode initial geometrical imperfections shapes, it becomes possible to compare the elastic post-buckling behaviors of columns containing them, in order to (i) obtain numerical evidence of the occurrence of G-G interaction and (ii) identify the most detrimental initial imperfection shape – this study considers initial imperfections corresponding to  $15^\circ$  intervals, *i.e.*,  $\theta=0\pm 15\pm 30\pm 45\pm 60\pm 75\pm 90^\circ$ .

The equilibrium paths  $P/P_{cr}$  vs.  $\gamma$  ( $\gamma$  is the mid-span torsional rotation) and  $P/P_{cr}$  vs.  $d_m/t$  ( $d_m$  is the mid-span translation due to minor-axis bending) displayed in Figs. 6(a<sub>1</sub>)-(a<sub>3</sub>) and 6(b<sub>1</sub>)-(b<sub>3</sub>), respectively, concern U<sub>6</sub> columns ( $\beta_{FT}=3.99$ ) with lengths  $L_1, L_5$  and  $L_7$  (*i.e.*, experiencing three different levels of G-G interaction –  $R_G=1.54; 1.12; 1.01$ ), and containing the 13 distinct initial geometrical imperfections dealt with in this work. As for Figs. 7(a)-(b), they show (i) four post-buckling equilibrium paths  $P/P_{cr}$  vs.  $\gamma$  and  $P/P_{cr}$  vs.  $d_m/t$ , already displayed in Fig. 6(a<sub>1</sub>)-(b<sub>1</sub>) and 6(a<sub>3</sub>)-(b<sub>3</sub>), concerning U<sub>6</sub> columns with lengths  $L_1$  or

<sup>4</sup> Since the column F<sub>M</sub>T post-buckling behavior is symmetric, it suffices to consider the half circle displayed in Fig. 5(a).

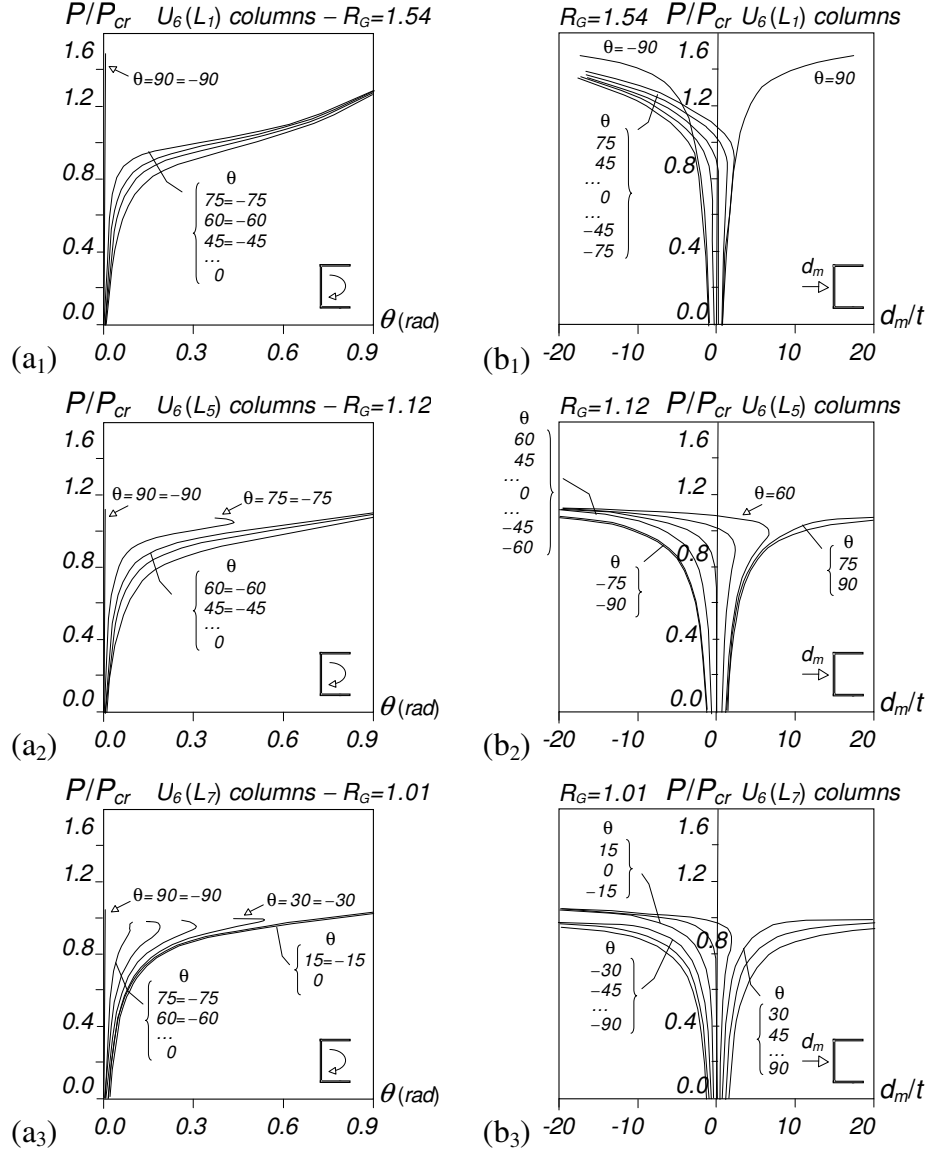


**Figure 6:** Elastic equilibrium paths (a)  $P/P_{cr}$  vs.  $\gamma$  and (b)  $P/P_{cr}$  vs.  $d_m/t$  of  $U_6$  columns with lengths (a)  $L_1$ , (b)  $L_5$  and (c)  $L_7$

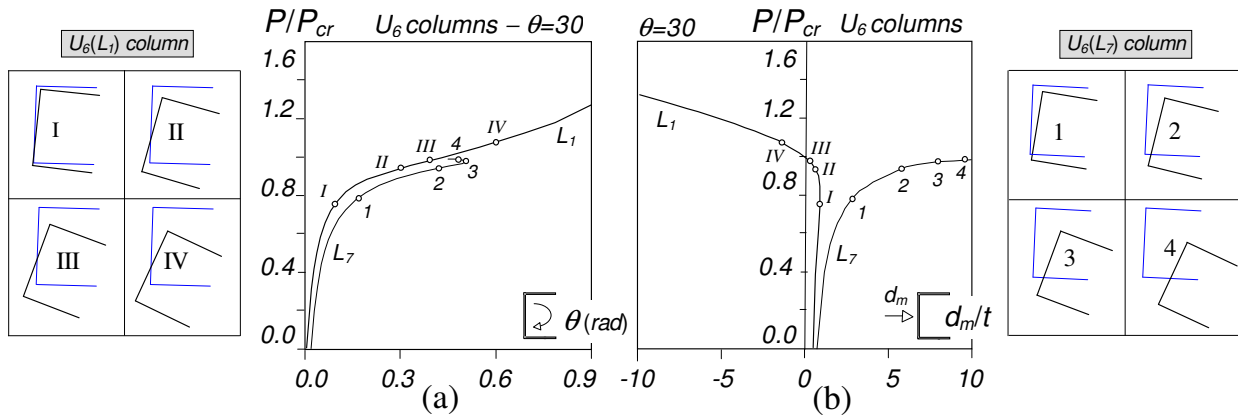


**Figure 7:**  $U_6$  columns with lengths  $L_1$  or  $L_7$  and  $\theta=30^\circ$  initial imperfections: elastic equilibrium paths (a)  $P/P_{cr}$  vs.  $\gamma$  and (b)  $P/P_{cr}$  vs.  $d_m/t$ , and mid-span cross-section deformed configuration evolution along those equilibrium paths

$L_7$  and  $\theta=30^\circ$  initial geometrical imperfections, and also (ii) the evolution of the column mid-span cross-section deformed configuration as loading progresses. The close observation of these post-buckling results prompts the following remarks:

- (i) The  $L_1$  column equilibrium paths  $P/P_{cr}$  vs.  $\gamma$  corresponding to  $\theta=0^\circ \pm 15^\circ \pm 30^\circ \pm 45^\circ \pm 60^\circ \pm 75^\circ$  exhibit the expected stable behavior and merge into a common curve, associated with clockwise mid-span torsional rotations. Their post-critical strengths are ordered according to the amplitude of the  $F_m$  initial imperfection component, *i.e.*, the lowest and highest post-critical strengths correspond to the  $\theta=0^\circ$  and  $\theta=\pm 75^\circ$  initial imperfections – naturally, the most detrimental initial imperfection shape is the “pure”  $F_{MT}$  one ( $\theta=0^\circ$ ). Moreover, the equilibrium paths  $P/P_{cr}$  vs.  $d_m/t$  of the five columns with positive  $\theta$  values exhibit a  $d_m$  reversal (from positive to negative) that occurs for  $P/P_{cr} \approx 0.85$  – this does not happen for the five columns with negative  $\theta$  values ( $d_m$  is always negative)<sup>5</sup>. As clearly shown by Dinis *et al.* (2020), by means of Generalized Beam Theory (GBT) geometrically non-linear analyses, this difference between the columns having positive and negative  $\theta$  values stems from effective centroid shift effects due to the stress redistribution occurring in the (singly symmetric) channel cross-section, caused mostly by the warping stresses. The weakening of the flanges moves the effective centroid closer to the web and the ensuing load eccentricity leads to negative (to the left)  $d_m$  translations that either oppose (columns with positive  $\theta$  values –  $d_m$  reversal) or reinforce (columns with negative  $\theta$  values – no  $d_m$  reversal) those coming from the initial imperfections.
- (ii) The  $L_1$  column  $P/P_{cr}$  vs.  $\gamma$  and  $P/P_{cr}$  vs.  $d_m/t$  equilibrium paths concerning  $\theta=90^\circ$  and  $\theta=-90^\circ$  (“pure”  $F_m$  initial geometrical imperfections) are identical and clearly different from the remaining ones – they correspond to a “singular” post-buckling behavior. Indeed, these columns exhibit virtually no  $F_{MT}$  deformations (only  $F_m$  ones) and their common post-critical strength is always the highest one – note that no effective centroid shift effects, due to the absence of  $F_{MT}$  deformations.
- (iii) The post-buckling behaviors of the  $L_5$  and  $L_7$  columns are markedly different from their  $L_1$  column counterpart, due to the fact that their  $R_G$  values are significantly lower (1.12 and 1.01 vs. 1.54). First of all, the post-critical strength is visibly smaller, which stems from the larger  $d_m$  values and reflects the presence of G-G ( $F_{MT}$ - $F_m$ ) interaction, naturally more relevant in the  $L_7$  columns – this interaction amplifies the  $d_m$  values due to the initial geometrical imperfections and effective centroid shifts. As before, the  $P/P_{cr}$  vs.  $\gamma$  and  $P/P_{cr}$  vs.  $d_m/t$  equilibrium paths concerning  $\theta=90^\circ$  and  $\theta=-90^\circ$  are identical and clearly different from the remaining ones. However, reflecting the strength erosion caused by the G-G interaction, their common post-critical strength is no longer the highest one – in fact, it is the lowest one for the  $L_7$  columns (even if this cannot be very clearly observed in Figs. 6(a<sub>3</sub>) and 6(b<sub>3</sub>)).
- (iv) In the  $L_5$  columns with  $\theta=\pm 75^\circ$  and the  $L_7$  columns with  $\theta=\pm 30^\circ \pm 45^\circ \pm 60^\circ \pm 75^\circ$ , the mid-span cross-section  $F_{MT}$  deformations cease to grow, rather abruptly, at a given applied load level, while the  $F_m$  deformations continue to grow – this means that the cross-section deformed configuration becomes progressively “more akin” to the  $F_m$  buckling mode shape. This feature is illustrated in Figs. 7(a)-(b), which compares the equilibrium paths and mid-span cross-section deformed configurations of the  $L_1$  and  $L_7$  columns with  $\theta=30^\circ$ . In the  $L_7$  column, note that the difference between the mid-span cross-section deformed configurations corresponding to the equilibrium states 3 and 4: while the  $F_{MT}$  deformations are practically the same, the  $F_m$  translations are quite different (the latter is much larger).
- (v) It can be concluded that, depending on the column  $R_G$  value, the most detrimental initial geometrical imperfection shape may be either the “pure”  $F_{MT}$  buckling mode ( $\theta=0^\circ$ ) or the “pure”  $F_m$  buckling mode ( $\theta=90^\circ$  or  $\theta=-90^\circ$ ). Since it is often impossible to know, beforehand, which is the most

<sup>5</sup> Obviously, the  $\theta=0^\circ$  column also does not exhibit  $d_m$  reversal, since  $d_m=0$  prior to  $P/P_{cr} \approx 0.85$ .

detrimental initial imperfection shape, it was decided to consider both of them in the parametric study presented in Section 5, intended to gather failure load data of columns buckling in  $F_{MT}$  modes.

- (vi) More in-depth knowledge on the mechanics of the coupling phenomenon under consideration in this work is currently being sought by the authors, through the GBT geometrically non-linear analysis of columns with various cross-section dimensions and undergoing several levels of G-G interaction ( $R_G$  values) – the outcome of this search/investigation will be reported in the near future.

#### 4.2 Elastic-Plastic Post-Buckling and Strength

As noted above, it was decided to determine failure loads concerning U columns containing both “pure”  $F_{MT}$  and “pure”  $F_m$  initial geometrical imperfections (amplitude  $L/1000$ ) – recall that, depending on the particular column under scrutiny, either failure load can be the lowest. In order to illustrate the type of results obtained, Figs. 8(a)-(b) show the elastic-plastic equilibrium paths  $P/P_{cr}$  vs.  $d_m/t$  of  $U_6$  columns with (i) lengths  $L_4, L_7$ , (ii) pure  $F_{MT}$  or  $F_m$  initial imperfections and (iii) three yield stresses ( $f_y/f_{cr,FT} \approx 1.2; 2.4; 3.5$  – the elastic equilibrium paths correspond to  $f_y/f_{cr,FT} = \infty$ ) – the failure loads obtained are identified by the white circles. Moreover, these figures also include the failure modes and plastic strains at collapse of the columns analyzed with  $f_y/f_{cr,FT} \approx 2.4$  – the failure modes corresponding to  $F_{MT}$  and  $F_m$  initial imperfections are identified by letters “A” and “B”, respectively, and have clearly visible features: while the former exhibits plastic strains at the mid-span and end cross-section top and bottom web-flange corner regions, the latter involves the full yielding of those cross-sections. The observation of these figures shows that:

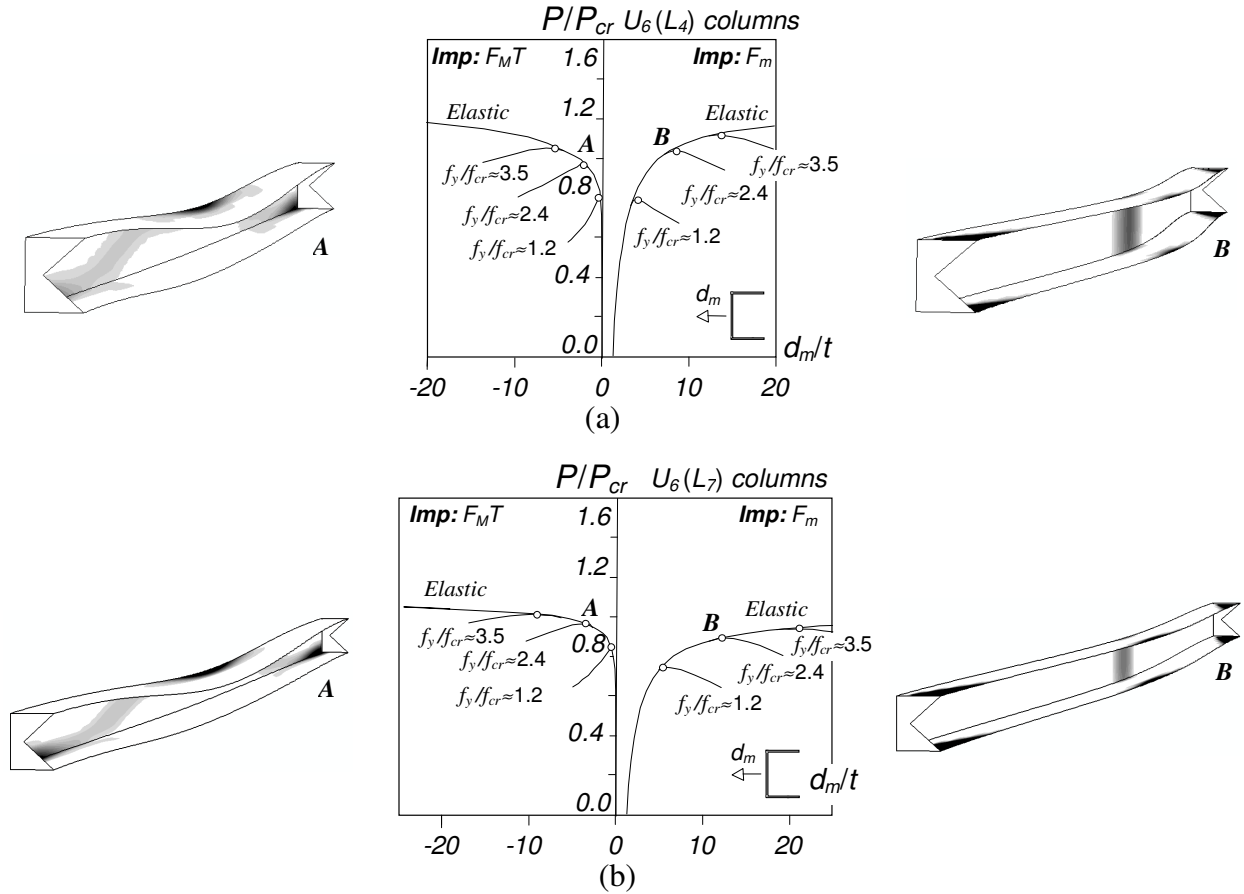


**Figure 8:** Elastic-plastic  $P/P_{cr}$  vs.  $d_m/t$  equilibrium paths and failure modes plus plastic strains at collapse ( $f_y/f_{cr,FT} \approx 2.4$ ) of  $U_6$  columns with lengths (a)  $L_4$  and (b)  $L_7$  with  $F_{MT}$  or  $F_m$  initial imperfections and yield stresses such that ( $f_y/f_{cr} \approx 1.2; 2.4; 3.5; \infty$ )

- (i) In the  $L_4$  columns, the failure loads obtained with  $F_{MT}$  initial imperfections are either a bit smaller ( $f_y/f_{cr,FT} \approx 2.4; 3.5$ ) or practically identical ( $f_y/f_{cr,FT} \approx 1.2$ ) to those concerning the  $F_m$  initial imperfections.
- (ii) In the  $L_7$  columns, conversely, the failure loads obtained with  $F_m$  initial imperfections are always visibly smaller than those concerning the  $F_{MT}$  initial imperfections. Unlike in the  $L_4$  columns, the difference is highest for  $f_y/f_{cr,FT} \approx 1.2$  and then decreases as the yield stress grows.

## 5. Failure Load Data for Columns Undergoing Global-Global Interaction

In order to be able to address the DSM-based design of fixed-ended cold-formed steel U columns affected by different levels of G-G interaction, it is indispensable to begin by gathering a reasonably extensive failure load set concerning columns under these circumstances. The failure loads obtained in this work correspond to columns with the 47 geometries (combinations of  $b_w$ ,  $b_f$ ,  $t$  and  $L$ ) given in Table 1, all associated with  $F_{MT}$  critical buckling, and five yield stresses,  $f_y=150; 300; 450; 600; 750$  MPa, enabling covering a wide critical slenderness range ( $\lambda_{FT}$ ). Although this equals a total of 235 different columns, 470 failure loads are determined, as each column is analyzed with two initial geometrical imperfections: “pure”  $F_{MT}$  and  $F_m$  imperfections – naturally, only the lowest one is retained for design purposes. The full set of failure loads obtained is presented, in tabular form, in Annex A.

## 6. DSM Design Considerations

Fig. 9(a) plots, against  $\lambda_{FT}$ , the  $P_u/P_{nFT}$  values obtained in this work – they are also given in the table included in Annex A. Fig. 9(b), on the other hand, plots the above  $P_u/P_{nFT}$  values, which concern columns with moderate and high slenderness ( $\lambda_{FT} > 1.5$ ), against the buckling load ratio  $R_G$  – its values are also given in the table of Annex A. Both figures include the associated  $P_u/P_{nFT}$  averages, standard deviations and maximum/minimum values. The observation of all these figures prompts the following remarks:

- (i) As anticipated (see Fig. 2), Eqs. (3)-(4) are unable to predict adequately the failure loads of the U columns affected by G-G mode interaction. Indeed, the  $P_u/P_{nFT}$  average (0.865), standard deviation (0.165) and minimum value (0.472) reflect a very poor prediction quality, combined with a very large percentage of failure load overestimations (74.0%). This quality falls even lower if only columns with  $\lambda_{FT} > 1.5$  are considered: the above indicators become 0.819, 0.153, 0.472 and 85.9%, respectively. Moreover, it is clear that the amount of failure load overestimation grows with  $\lambda_{FT}$ .
- (ii) As also anticipated, Fig. 9(b) clearly shows that the amount of failure load overestimation is closely linked to the buckling load ratio  $R_G$  values – indeed, it is highest for  $R_G \approx 1.0$ , it remains meaningful up to  $R_G \approx 1.5$  and practically ceases to occur for  $R_G > 1.5$ .

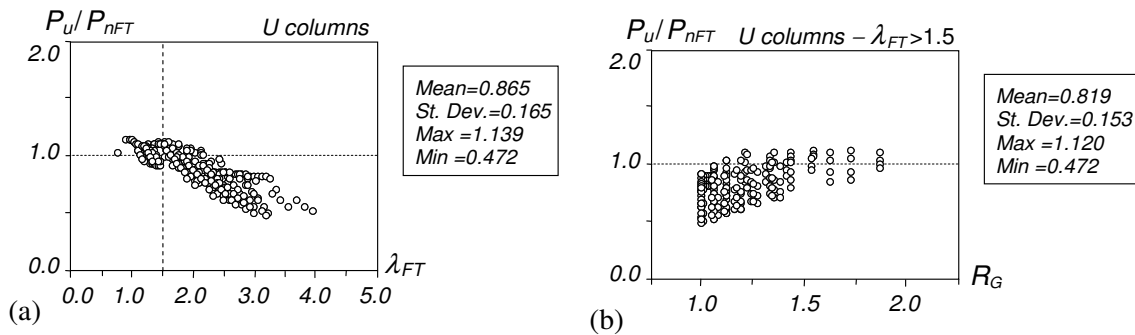


**Figure 9:** Plots (a)  $P_u/P_{nFT}$  vs.  $\lambda_{FT}$ , for all the columns analyzed, and (b)  $P_u/P_{nFT}$  vs.  $R_G$ , for the columns with  $\lambda_{FT} > 1.5$

In view of (i) the very poor failure load prediction quality reflected in Fig. 9(a) and (ii) the important role played by the G-G interaction in this poor performance (see Fig. 9(b)), it was decided to look for fresh insight on these column behavioral features, with the goal of searching for a DSM-based design approach that can handle adequately U column G-G interactive failures. The first step towards reaching this goal is to group the available  $P_u/P_y$  values according to the corresponding  $\beta_{FT}$  and  $R_G$  values – the latter correlates very well with the column length. Figs. 10(a)-(g) plot, against  $\lambda_{FT}$ , the  $P_u/P_y$  values concerning the  $U_6$  columns ( $\beta_{FT}=3.99$ ) with lengths  $L_1-L_7$  ( $R_G=1.54; 1.42; 1.32; 1.22; 1.12; 1.07; 1.01$ , respectively), and compares them with the corresponding DSM design curve ( $P_{nFT}$ ). The figures include the column failure loads obtained with the  $F_{MT}$  and  $F_m$  initial imperfections ( $P_{u,FT}$  and  $P_{u,Fm}$  – white and grey circles, respectively). The observation of all these figures prompts the following remarks:

- (i) The  $L_1$  columns exhibit the expected  $F_{MT}$ :  $P_{u,FT}$  are always the lowest failure loads and they are efficiently (safely and accurately) predicted by  $P_{nFT}$  strength curve provided by Eqs. (3)-(4).
- (ii) However, in spite of the relatively high  $R_G$  value ( $R_G=1.54$ ), the failure loads of the most slender ( $\lambda_{FT}>2.0$ )  $L_1$  columns are slightly affected by G-G interaction emerging and developing only at the

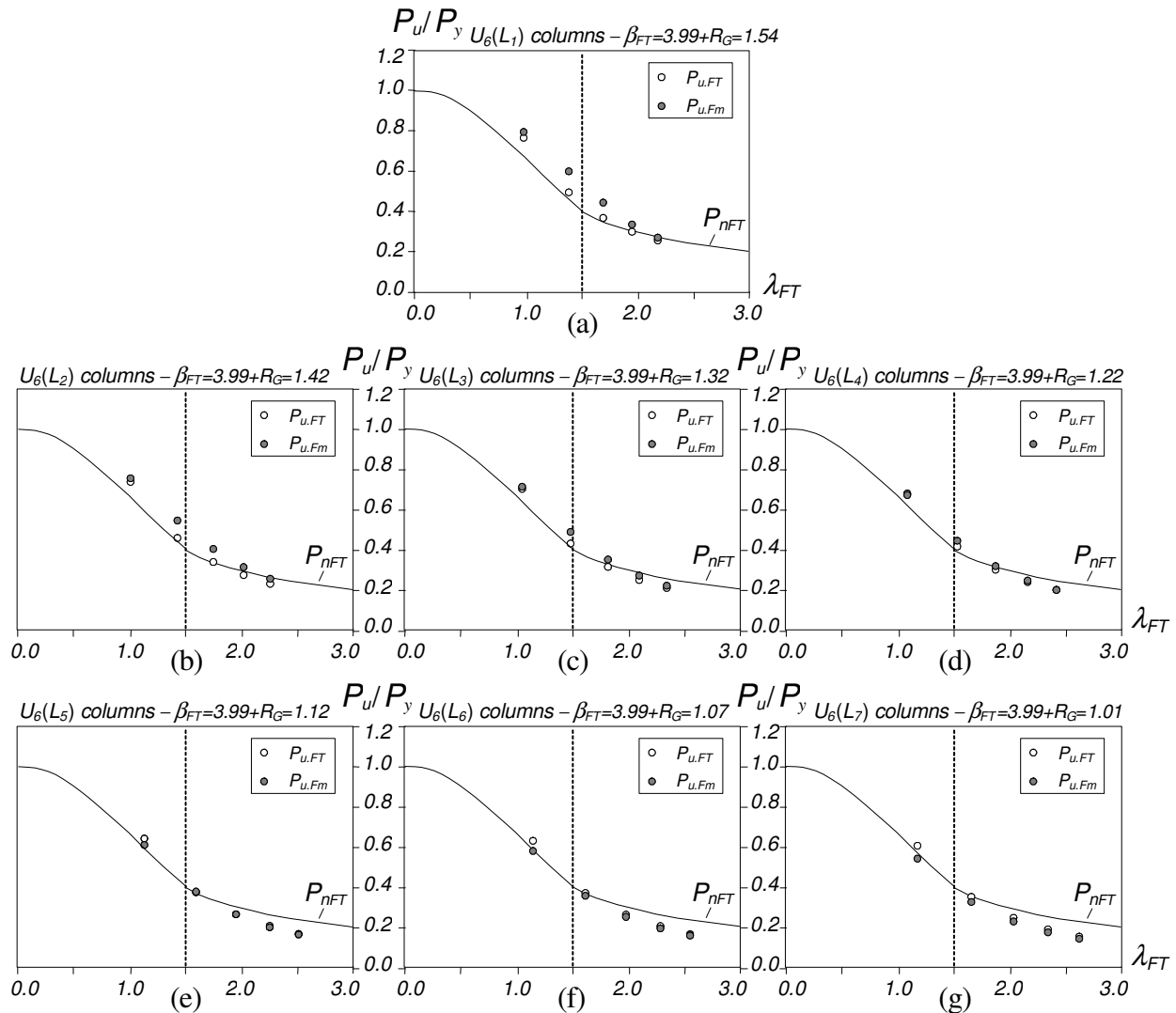


**Figure 10:** Comparison between the DSM strength curve ( $P_{nFT}/P_y$ ) and the  $P_{u,FT}/P_y$  and  $P_{u,Fm}/P_y$  values of  $U_6$  columns ( $\beta_{FT}=3.99$ ) with (a)  $L_1$ , (b)  $L_2$ , (c)  $L_3$ , (d)  $L_4$ , (e)  $L_5$ , (f)  $L_6$  and (g)  $L_7$  lengths

advanced post-buckling stages (termed here “secondary G-G interaction”). This is confirmed by the fact that their  $P_{u,FT}/P_{nFT}$  values are 0.98 and 0.93, *i.e.*, correspond to slight overestimations. Another sign of the occurrence of secondary G-G interaction is the progressive closeness between the  $P_{u,FT}$  and  $P_{u,Fm}$  values as the column slenderness increases.

- (iii) As it would be logical to expect, increasing the column length (*i.e.*, decreasing  $R_G$ ) leads to stronger G-G interaction effects, particularly in the moderate and high slenderness range ( $\lambda_{FT} > 1.5$ ), which corresponds to the columns with the three largest yield stresses. This is attested by the sequence of trios of  $P_{u,FT}/P_{nFT}$  values concerning columns with the same length: 1.02;0.94;0.89 ( $L_2 - R_G=1.42$ ), 0.98;0.90;0.84 ( $L_3 - R_G=1.32$ ), 0.95;0.86;0.79 ( $L_4 - R_G=1.22$ ), 0.89;0.79;0.71 ( $L_5 - R_G=1.12$ ), 0.84;0.74;0.67 ( $L_6 - R_G=1.07$ ) 0.77;0.68;0.61 ( $L_7 - R_G=1.01$ ) – naturally, the level of overestimation increases with the slenderness, *i.e.*, the yield stress. Finally, it is still worth noting that, in the columns with  $L_5$ ,  $L_6$  and  $L_7$  strengths, the  $P_{u,Fm}$  failure loads become smaller than the  $P_{u,FT}$  ones, thus further increasing the level of overestimation provided by the  $P_{nFT}$  strength curve.

A similar investigation was carried out for columns with larger  $\beta_{FT}$  values. Figs. 11(a)-(c) plot, against  $\lambda_{FT}$ , the  $P_{u,FT}/P_y$  and  $P_{u,Fm}/P_y$  values concerning  $U_1$  columns ( $\beta_{FT}=18.13$ ) with lengths  $L_1$ ,  $L_4$  and  $L_7$  ( $R_G=1.06$ ; 1.03; 1.01), and compare them with the corresponding DSM strength curve ( $P_{nFT}/P_y$ ). The observation of these figures leads to the following remarks:

- (i) The  $P_{u,FT}/P_y$  and  $P_{u,Fm}/P_y$  “clouds” are very similar for the three column sets. In fact, the  $P_{u,FT}/P_y$  and  $P_{u,Fm}/P_y$  values are well aligned along the  $P_{nFT}/P_y$  curve. However, it is also noted that all the  $P_{u,Fm}$  values are always lower than the  $P_{nFT}$  ones. Moreover, all  $P_{u,FT}/P_y$  values are above the  $P_{nFT}/P_y$  curve, while precisely the opposite happens for the  $P_{u,Fm}/P_y$  values (all below that curve).
- (ii) Increasing the column length (*i.e.*, decreasing  $R_G$ ) has no visible impact on the failure load prediction quality provided by the  $P_{nFT}$  values. For the three lengths considered, the ratio  $P_{u,Fm}/P_{nFT}$  varies between 0.88 and 0.80 – the level of overestimation grows slightly with the slenderness.
- (iii) The contents of the previous items are consistent with the fact that all columns exhibit very low  $R_G$  values ( $1.06 \geq R_G \geq 1.00$ ), *i.e.*, are strongly affected by (“true”) G-G interaction.

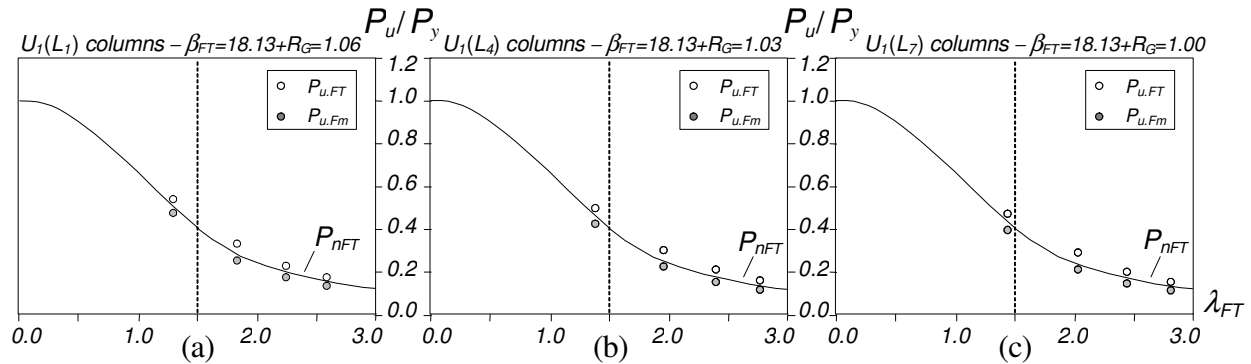


**Figure 11:** Comparison between the DSM strength curve ( $P_{nFT}/P_y$ ) and the  $P_{u,FT}/P_y$  and  $P_{u,Fm}/P_y$  values of  $U_1$  columns ( $\beta_{FT}=18.13$ ) with (a)  $L_1$ , (b)  $L_4$  and (c)  $L_7$  lengths

### 6.1 DSM-Based Design Approach Able to Handle Column Global-Global Interactive Failures

The aim of this section is to extend the scope of the DSM-based strength curve proposed by Dinis *et al.* (2020), developed in the context of fixed-ended U columns unaffected by G-G interaction (large  $R_G$  values), making it capable of handling also U column G-G interactive failures. In other words, to develop

a DSM-based design approach that can predict adequately the failure loads of fixed-ended U columns buckling in  $F_{MT}$  modes, regardless of their  $R_G$  values. Following a strategy practically identical to that adopted by Dinis *et al.* (2020), a modification of the existing  $\beta_{FT}$ -dependent strength curve set is sought, so that G-G interactive failure can also be adequately handled. After grouping all the fixed-ended U columns analyzed in this work and previously (Dinis *et al.* 2019, 2020) according to their  $\beta_{FT}$  values, a “trial-and-error curve-fitting procedure” led to a new expression for parameter  $b$  (see Eq. (4)), which now depends not only on  $\beta_{FT}$ , but also on  $R_G$ , via a new additive parameter  $c$ . The proposed strength curve set, termed here  $P_{nFT-G}$ , is defined by the expressions

$$P_{nFT-G} = \begin{cases} f_y \left( 0.658 \lambda_{FT}^2 \right) & \text{if } \lambda_{FT} \leq 1.5 \\ f_y \left( \frac{a}{\lambda_{FT}^b} \right) & \text{if } \lambda_{FT} > 1.5 \end{cases} \quad \text{with} \quad \lambda_{FT} = \sqrt{\frac{P_y}{P_{crFT}}} \quad , \quad (5)$$

$$a = 0.39 \times 1.5^b \quad , \quad (6)$$

$$b = 0.06 \beta_{FT} + c \leq 2.0 \quad , \quad (7)$$

$$c = -19.5 R_G^3 + 73.6 R_G^2 - 94.1 R_G + 42 \geq 0.71 \quad , \quad (8)$$

where  $\beta_{FT}$  is still given by Eq. (2) and recall that  $R_G = P_{b,Fm} / P_{cr,FT}$ . Note that Eqs. (3)-(4) are recovered for  $R_G \geq 1.49$  (one has then  $c=0.71$ ), which means that the fixed-ended U column failure load prediction quality achieved by Dinis *et al.* (2020) remains unaltered.

In order to illustrate the failure load prediction quality achieved by the modified strength curve set, for the columns affected by G-G interaction considered in this work, Figs. 12(a)-(f) plot, against  $\lambda_{FT}$ , the

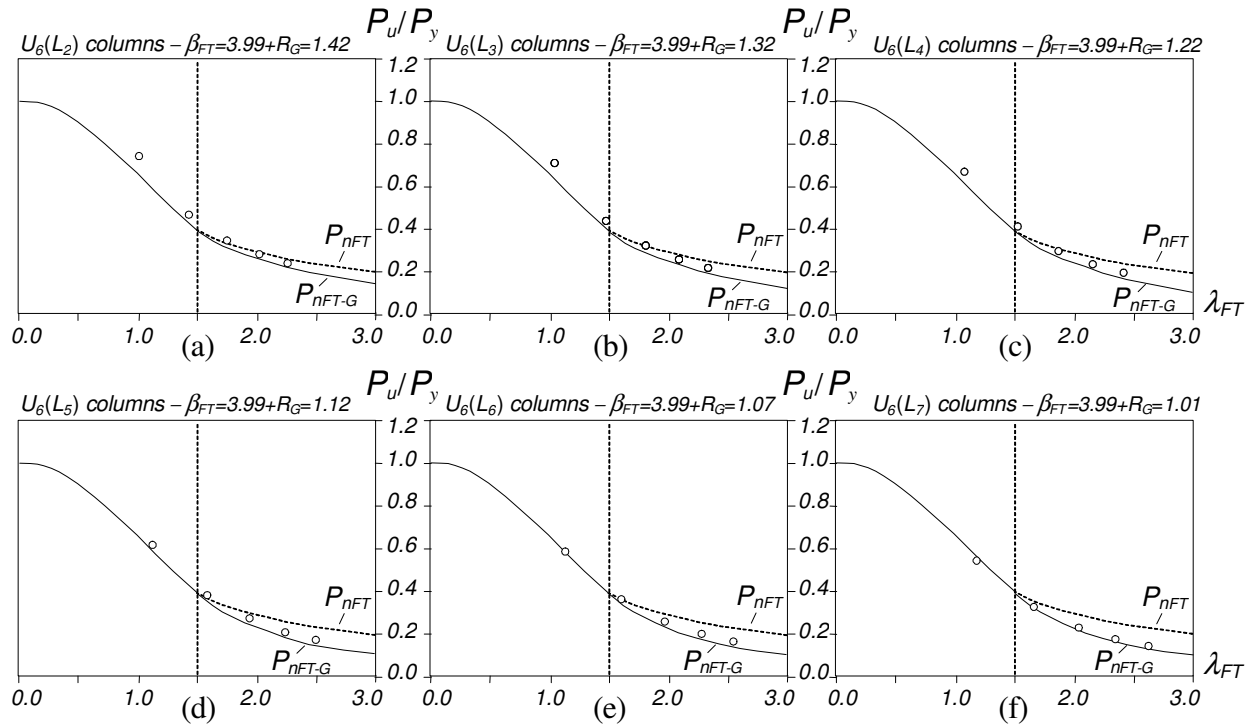


**Figure 12:** Comparison between the proposed DSM strength curve set ( $P_{nFT-G}/P_y$ ) and the  $P_{u,min}/P_y$  values of  $U_6$  columns with (a)  $L_2$ , (b)  $L_3$ , (c)  $L_4$ , (d)  $L_5$ , (e)  $L_6$  and (f)  $L_7$  lengths

$P_u/P_y$  values ( $P_u$  is the lowest of the failure loads  $P_{u,FT}$  and  $P_{u,Fm}$ ) concerning the U<sub>6</sub> columns ( $\beta_{FT}=3.99$ ) with lengths  $L_2-L_7$  ( $R_G=1.42; 1.32; 1.22; 1.12; 1.07; 1.01$ ), and compare them with the DSM-based strength curves set defined by Eqs. (3)-(4) and (5)-(8) ( $P_{nFT}$  and  $P_{nFT-G}$  – dashed and solid lines, respectively). It is clear that all  $P_u/P_y$  values are quite well predicted by the  $P_{nFT-G}/P_y$  strength curves – indeed, they invariably provide rather accurate failure underestimations, regardless of the G-G interaction level.

The table included in Annex A provides the numerical failure-to-predicted failure load ratios  $P_{u,FT}/P_{nFT-G}$  and  $P_{u,Fm}/P_{nFT-G}$  concerning the U columns analyzed in this work, as well as the values of the relevant quantities involved in their calculation, namely the column buckling load ratios  $R_G$ . In order to assess the performance and merits of the proposed strength curve set, Fig. 13(a) plots, against  $\lambda_{FT}$ , the  $P_u/P_{nFT-G}$  values concerning all these U columns, almost all of them affected by G-G interaction. As for Fig. 13(b), it plots, again vs.  $\lambda_{FT}$ , the  $P_u/P_{nFT-G}$  concerning the fixed-ended U column failure loads reported by Dinis *et al.* (2020), whose  $R_G$  values are all much higher than 1.0 ( $R_G \geq 1.45$ ). Both figures include the associated  $P_u/P_{nFT-G}$  averages, standard deviations and maximum/minimum values. Finally, Table 2 provides, for the various fixed-ended U column sets, the failure load numbers ( $n$ ) and  $P_u/P_{nFT-G}$  statistical indicators, making a distinction between the columns with  $\lambda_{FT} \leq 1.5$  and  $\lambda_{FT} > 1.5$ . The observation of the results presented in the above figures and table prompts the following remarks:

- (i) The proposed DSM-based column strength curve set, dependent on  $\beta_{FT}$  and  $R_G$ , provides high-quality failure load predictions for the U columns affected by G-G interaction. Indeed, the  $P_u/P_{nFT-G}$  averages, standard deviations and maximum/minimum values are 1.038-0.078-1.182-0.850. For  $\lambda_{FT} \leq 1.5$  and  $\lambda_{FT} > 1.5$ , these indicators are 1.033-0.069-1.139-0.905 and 1.034-0.078-1.182-0.850, respectively, which means that the failure load prediction quality is quite similar in both slenderness ranges – in the whole slenderness range, one has 1.038-0.078-1.182-0.850.

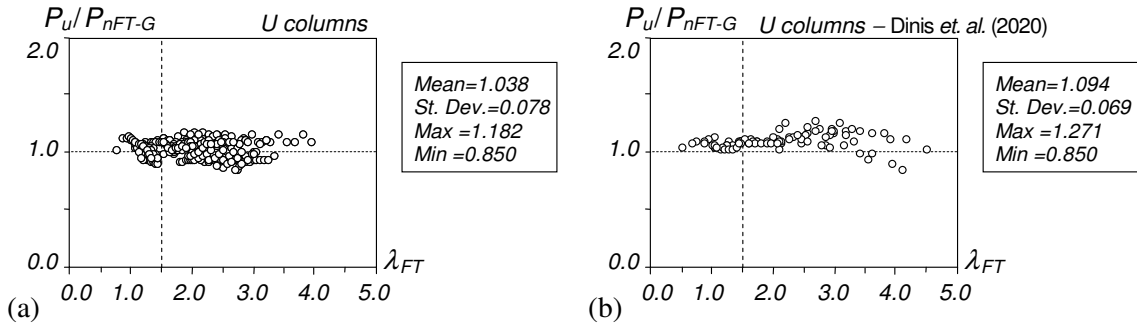


**Figure 13:** Plots  $P_u/P_{nFT-G}$  vs.  $\lambda_{FT}$ , for all the U columns (a) analyzed in this work and (b) reported by Dinis *et al.* (2020)

**Table 2:** Statistical indicators of the  $P_u/P_{nFT-G}$  values concerning the failure loads of the fixed-ended U columns analyzed in this work, reported by Dinis *et al.* (2020) and both combined

U Columns	This work		Dinis <i>et al.</i> (2020)		All columns	
	$\leq 1.5$	$> 1.5$	$\leq 1.5$	$> 1.5$	$\leq 1.5$	$> 1.5$
$\lambda_{FT}$						
$n$	51	184	29	61	80	245
Mean	1.033	1.034	1.056	1.108	1.044	1.053
Sd. Dev.	0.069	0.078	0.028	0.078	0.059	0.084
Max	1.139	1.182	1.125	1.271	1.139	1.271
Min	0.905	0.850	1.017	0.850	0.905	0.850

- (ii) Since the DSM-based column strength curves proposed in this work coincide with those developed by Dinis *et al.* (2020) for  $R_G \geq 1.49$ , it is not surprising that the failure load prediction quality remains unaltered (and excellent) for the U columns reported by those authors. Indeed, the statistical indicators of their  $P_u/P_{nFT-G}$  are 1.056-0.028-1.125-0.850 and 1.108-0.078-1.271-0.850, respectively for  $\lambda_{FT} \leq 1.5$  and  $\lambda_{FT} > 1.5$  – in the whole slenderness range, one has 1.094-0.069-1.271-0.850.
- (iii) In view of the content of the two previous items, it can be rightfully stated that the proposed DSM-based column strength curve set (see Eqs. (5)-(8)) ensures a high prediction quality for the numerical failure loads of all the fixed-ended U columns buckling in  $F_{MT}$  modes analyzed so far, regardless of their  $\beta_{FT}$  and  $R_G$  value combinations.

## 7. Conclusion

This work reported the available numerical results of an ongoing investigation dealing with the post-buckling behavior, strength and DSM design of cold-formed steel columns buckling in  $F_{MT}$  modes and undergoing global-global (G-G) interaction – the results presented and discussed in the paper concern exclusively fixed-ended plain channel (U) columns and constitute the first step of this research effort. After a brief overview of the main features and merits of the DSM-based design approach proposed by Dinis *et al.* (2020) to predict column  $F_{MT}$  failure loads, the paper addressed the column buckling behavior in order to select column geometries susceptible to the occurrence of various levels of G-G interaction. Then, following an investigation on the elastic and elastic-plastic post-buckling behavior and strength of the columns under consideration, which included the identification of the most detrimental critical-mode initial geometrical imperfection shape, the paper assembled  $F_{MT}$  failure load data obtained by means of a parametric study involving the selected columns with several yield stresses, chosen to enable covering a wide slenderness range. Finally, the assembled numerical  $F_{MT}$  failure load data were used (i) to show that the DSM-based strength curve set proposed by Dinis *et al.* (2020) is unable to adequately predict them and (ii) as the basis to search for an improved DSM-based design approach able to handle also G-G interactive failures of columns buckling in  $F_{MT}$  modes. This search was shown to be successful and led to a modification of the column strength curve set proposed by Dinis *et al.* (2020) – it consists of incorporating the buckling load ratio  $R_G$  in the expressions providing the strength curves, thus accounting for the level of G-G interaction. The modified/improved DSM-based design approach was shown (i) to predict quite adequately (safely and accurately) the failure loads of the fixed-ended U columns, buckling in  $F_{MT}$  modes and affected by G-G interaction, considered in this work and, at the same time, (ii) to retain the high failure load prediction quality for the columns unaffected by this interaction, namely those reported by Dinis *et al.* (2019, 2020).

Although this work was restricted to fixed-ended U columns, the quality of the findings reported provides strong encouragement to proceed along this path, as the methodology adopted is expected to bear fruits also for columns with other cross-section shapes and/or end support conditions. Indeed, the authors are currently investigating (i) fixed-ended lipped channel (C) and (ii) pin-ended U columns – the outcomes of these investigation will be reported in the near future.

## References

- AISC (American Institute of Steel Construction) (1986). *Load and Resistance Factor Design Specification for Structural Steel Buildings* (AISC 328:1986), Chicago IL.
- ISI (American Iron and Steel Institute) (1986). *Cold-Formed Steel Design Manual*, Washington DC.
- ISI (American Iron and Steel Institute) (1996). *Cold-Formed Steel Design Manual*, Washington DC.

- Bebiano R, Camotim D, Gonçalves R (2018). GBTUL 2.0 – a second-generation code for the GBT-based buckling and vibration analysis of thin-walled members, *Thin-Walled Structures*, **124**(March), 235-257.
- Camotim D., Dinis P.B. (2011). Coupled instabilities with distortional buckling in cold-formed steel lipped channel columns, *Thin-Walled Structures*, **49**(5), 562-575.
- Camotim D, Dinis PB, Martins AD. (2016). Direct Strength Method (DSM) – a general approach for the design of cold-formed steel structures, *Recent Trends in Cold-Formed Steel Construction*, C. Yu (ed.), Woodhead Publishing (Amsterdam – Series in Civil and Structural Engineering), 69-105.
- Camotim D., Dinis P.B., Landesmann A. (2019). Behavior, failure and Direct Strength Method design of steel angle columns: geometrical simplicity vs. structural complexity, *submitted for publication*.
- Dinis P.B., Camotim D. (2015). A novel DSM-based approach for the rational design of fixed-ended and pin-ended short-to-intermediate thin-walled angle columns, *Thin-Walled Structures*, **87**(February), 158-182.
- Dinis P.B., Camotim D., Silvestre N. (2012). On the mechanics of thin-walled angle column instability, *Thin-Walled Structures*, **52**(March), 80-89.
- Dinis PB, Camotim D, Landesmann A, Martins AD (2019). On the Direct Strength Method design of columns against global failure, *Thin-Walled Structures*, **139**(June), 242-270.
- Dinis P.B., Camotim D., Landesmann A., Martins A.D. (2020). Improving the Direct Strength Method prediction of column flexural-torsional failure loads, *Thin-Walled Structures*, in press.
- Ellobody E., Young B. (2005). Behavior of cold-formed steel plain angle columns, *Journal of Structural Engineering* (ASCE), **131**(3), 469-478.
- Hancock G.J., Kwon Y.B., Bernard E.S. (1994). Strength design curves for thin-walled sections undergoing distortional buckling, *Journal of Construction Steel Research*, **31**(2-3), 169-186.
- Li Z., Abreu J.C.B., Leng J., Ádány S., Schafer B.W. (2014). Review: constrained finite strip method developments and applications in cold-formed steel design, *Thin-Walled Structures*, **81**(August), 2-18.
- Peköz T, Sümer O (1992), *Design Provisions for Cold-Formed Steel Columns and Beam-Column*, Research Report RP92-1, American Iron and Steel Institute, Washington DC.
- Schafer B.W. (2008). Review: the direct strength method of cold-formed steel member design, *Journal of Constructional Steel Research*, **64**(7-8), 766-778.
- Schafer B.W. (2019). Advances in the Direct Strength Method of cold-formed steel design, *Thin-Walled Structures*, **140**(July), 533-541.
- Schafer BW, Peköz T (1998). Direct strength prediction of cold-formed steel members using numerical elastic buckling solutions, *Proceedings of 14<sup>th</sup> International Specialty Conference on Cold-Formed Steel Structures* (St. Louis, 15-16/10), W.W. Yu, R. LaBoube (eds.), 69-76.
- Torabian S., Schafer B.W. (2018). Development and experimental validation of the Direct Strength Method for cold-formed steel beam-columns, *Journal of Structural Engineering* (ASCE), **144**(10), paper 04018175 (21 pages).
- Ziemian R (editor) (2010). *Guide to Stability Design Criteria for Metal Structures* (6<sup>th</sup> edition), John Wiley & Sons, Hoboken.

## ANNEX A

**Table A1:** U Columns failing in  $F_{MT}$  modes: (i) geometries, (ii) buckling stresses and failure loads, (iii) failure load predictions by existing and proposed DSM design curve sets, and (iv) numerical-to-predicted failure loads ratios (mm, MPa, kN)

Column	Geometry			SFEA					DSM Design												
	$b_w \times b_f \times t$	$\beta_{FT}$	$L$	$f_y$	$P_{u,FT}$	$P_{u,Fm}$	$P_u$	$f_{cr,FT}$	$\lambda_{FT}$	$b$	$a$	$P_{n,FT}$	$\frac{P_u}{P_{n,FT}}$	$f_{cr,Fm}$	$R_G$	$c$	$b$	$a$	$P_{n,FT-G}$	$\frac{P_u}{P_{n,FT-G}}$	
U1_L1	100x40x1.2	18.13	3700	150	17.1	15.0	15.0	89.7	1.29	1.80	0.81	16.1	0.93	95.4	1.06	1.71	2.00	0.88	16.1	0.93	
		18.13	3700	300	20.7	15.6	15.6	89.7	1.83	1.80	0.81	17.7	0.88	95.4	1.06	1.71	2.00	0.88	17.0	0.92	
		18.13	3700	450	20.8	15.6	15.6	89.7	2.24	1.80	0.81	18.4	0.84	95.4	1.06	1.71	2.00	0.88	17.0	0.92	
		18.13	3700	600	20.8	15.6	15.6	89.7	2.59	1.80	0.81	19.0	0.82	95.4	1.06	1.71	2.00	0.88	17.0	0.92	
U1_L2	100x40x1.2	18.13	3700	750	20.8	15.6	15.6	89.7	2.89	1.80	0.81	19.4	0.80	95.4	1.06	1.71	2.00	0.88	17.0	0.92	
		18.13	3800	150	16.6	14.5	14.5	85.9	1.32	1.80	0.81	15.6	0.93	90.5	1.05	1.75	2.00	0.88	15.6	0.93	
		18.13	3800	300	20.3	15.1	15.1	85.9	1.87	1.80	0.81	17.0	0.88	90.5	1.05	1.75	2.00	0.88	16.3	0.92	
		18.13	3800	450	20.4	15.1	15.1	85.9	2.29	1.80	0.81	17.7	0.85	90.5	1.05	1.75	2.00	0.88	16.3	0.92	
U1_L3	100x40x1.2	18.13	3800	600	20.4	15.1	15.1	85.9	2.64	1.80	0.81	18.3	0.82	90.5	1.05	1.75	2.00	0.88	16.3	0.92	
		18.13	3800	750	20.4	15.1	15.1	85.9	2.95	1.80	0.81	18.7	0.81	90.5	1.05	1.75	2.00	0.88	16.3	0.92	
		18.13	3900	150	16.2	14.0	14.0	82.4	1.35	1.80	0.81	15.1	0.92	86.0	1.04	1.79	2.00	0.88	15.1	0.92	
		18.13	3900	300	19.7	14.5	14.5	82.4	1.91	1.80	0.81	16.4	0.89	86.0	1.04	1.79	2.00	0.88	15.6	0.93	
U1_L4	100x40x1.2	18.13	3900	450	20.1	14.5	14.5	82.4	2.34	1.80	0.81	17.1	0.85	86.0	1.04	1.79	2.00	0.88	15.6	0.93	
		18.13	3900	600	20.1	14.5	14.5	82.4	2.70	1.80	0.81	17.6	0.83	86.0	1.04	1.79	2.00	0.88	15.6	0.93	
		18.13	3900	750	20.1	14.5	14.5	82.4	3.02	1.80	0.81	18.0	0.81	86.0	1.04	1.79	2.00	0.88	15.6	0.93	
		18.13	4000	150	15.8	13.5	13.5	79.1	1.38	1.80	0.81	14.7	0.92	81.7	1.03	1.84	2.00	0.88	14.7	0.92	
U1_L5	100x40x1.2	18.13	4000	300	18.9	14.0	14.0	79.1	1.95	1.80	0.81	15.8	0.89	81.7	1.03	1.84	2.00	0.88	15.0	0.93	
		18.13	4000	450	19.7	14.0	14.0	79.1	2.39	1.80	0.81	16.5	0.85	81.7	1.03	1.84	2.00	0.88	15.0	0.93	
		18.13	4000	600	19.7	14.0	14.0	79.1	2.75	1.80	0.81	17.0	0.83	81.7	1.03	1.84	2.00	0.88	15.0	0.93	
		18.13	4000	750	19.7	14.0	14.0	79.1	3.08	1.80	0.81	17.3	0.81	81.7	1.03	1.84	2.00	0.88	15.0	0.93	
U1_L6	100x40x1.2	18.13	4100	150	15.4	13.0	13.0	76.0	1.40	1.80	0.81	14.2	0.92	77.8	1.02	1.88	2.00	0.88	14.2	0.92	
		18.13	4100	300	18.7	13.5	13.5	76.0	1.99	1.80	0.81	15.2	0.89	77.8	1.02	1.88	2.00	0.88	14.4	0.94	
		18.13	4100	450	18.7	13.5	13.5	76.0	2.43	1.80	0.81	15.9	0.85	77.8	1.02	1.88	2.00	0.88	14.4	0.94	
		18.13	4100	600	18.7	13.5	13.5	76.0	2.81	1.80	0.81	16.4	0.83	77.8	1.02	1.88	2.00	0.88	14.4	0.94	
U1_L7	100x40x1.2	18.13	4100	750	18.7	13.5	13.5	76.0	3.14	1.80	0.81	16.7	0.81	77.8	1.02	1.88	2.00	0.88	14.4	0.94	
		18.13	4200	150	15.0	12.5	12.5	73.3	1.43	1.80	0.81	13.8	0.91	74.2	1.01	1.94	2.00	0.88	13.8	0.91	
		18.13	4200	300	18.2	13.0	13.0	73.3	2.02	1.80	0.81	14.8	0.88	74.2	1.01	1.94	2.00	0.88	13.9	0.94	
		18.13	4200	450	18.5	13.0	13.0	73.3	2.48	1.80	0.81	15.4	0.85	74.2	1.01	1.94	2.00	0.88	13.9	0.94	
U1_L8	100x40x1.2	18.13	4200	600	18.5	13.0	13.0	73.3	2.86	1.80	0.81	15.8	0.82	74.2	1.01	1.94	2.00	0.88	13.9	0.94	
		18.13	4200	750	18.5	13.0	13.0	73.3	3.20	1.80	0.81	16.2	0.81	74.2	1.01	1.94	2.00	0.88	13.9	0.94	
		18.13	4300	150	14.6	12.1	12.1	70.6	1.46	1.80	0.81	13.3	0.91	70.8	1.00	1.98	2.00	0.88	13.3	0.91	
		18.13	4300	300	17.8	12.6	12.6	70.6	2.06	1.80	0.81	14.3	0.88	70.8	1.00	1.98	2.00	0.88	13.4	0.94	
U1_L9	100x40x1.2	18.13	4300	450	18.0	12.6	12.6	70.6	2.52	1.80	0.81	14.9	0.85	70.8	1.00	1.98	2.00	0.88	13.4	0.94	
		18.13	4300	600	18.0	12.6	12.6	70.6	2.92	1.80	0.81	15.3	0.82	70.8	1.00	1.98	2.00	0.88	13.4	0.94	
		18.13	4300	750	18.0	12.6	12.6	70.6	3.26	1.80	0.81	15.7	0.80	70.8	1.00	1.98	2.00	0.88	13.4	0.94	
		18.13	4300	150	14.6	12.1	12.1	70.6	1.46	1.80	0.81	13.3	0.91	70.8	1.00	1.98	2.00	0.88	13.3	0.91	
U2_L1	100x40x2.0	14.85	2200	150	46.4	42.8	42.8	252.9	0.77	1.60	0.75	42.1	1.02	268.4	1.06	1.72	2.00	0.88	42.1	1.02	
		14.85	2200	300	73.4	68.0	68.0	252.9	1.09	1.60	0.75	65.7	1.04	268.4	1.06	1.72	2.00	0.88	65.7	1.04	
		14.85	2200	450	84.2	77.8	77.8	252.9	1.33	1.60	0.75	76.9	1.01	268.4	1.06	1.72	2.00	0.88	76.9	1.01	
		14.85	2200	600	90.0	78.8	78.8	252.9	1.54	1.60	0.75	80.7	0.98	268.4	1.06	1.72	2.00	0.88	79.9	0.99	
U2_L2	100x40x2.0	14.85	2200	750	93.2	78.8	78.8	252.9	1.72	1.60	0.75	84.4	0.93	268.4	1.06	1.72	2.00	0.88	79.9	0.99	
		8.48	4000	150	41.4	48.4	41.4	115.9	1.14	1.22	0.64	38.4	1.08	200.5	1.73	0.71	1.22	0.64	38.4	1.08	
		8.48	4000	300	52.4	59.0	52.4	115.9	1.61	1.22	0.64	47.3	1.11	200.5	1.73	0.71	1.22	0.64	47.3	1.11	
		8.48	4000	450	61.2	59.0	59.0	115.9	1.97	1.22	0.64	55.4	1.06	200.5	1.73	0.71	1.22	0.64	55.4	1.06	
U2_L3	100x40x2.0	8.48	4000	600	67.8	59.0	59.0	115.9	2.28	1.22	0.64	62.0	0.95	200.5	1.73	0.71	1.22	0.64	62.0	0.95	
		8.48	4000	750	72.6	59.0	59.0	115.9	2.54	1.22	0.64	67.6	0.87	200.5	1.73	0.71	1.22	0.64	67.6	0.87	
		8.48	4500	150	36.8	43.7	36.8	97.0	1.24	1.22	0.64	34.6	1.06	158.3	1.63	0.71	1.22	0.64	34.6	1.06	
		8.48	4500	300	46.6	51.9	46.6	97.0	1.76	1.22	0.64	42.4	1.10	158.3	1.63	0.71	1.22	0.64	42.4	1.10	
U2_L4	100x40x2.0	8.48	4500	450	54.6	51.9	51.9	97.0	2.15	1.22	0.64	49.7	1.04	158.3	1.63	0.71	1.22	0.64	49.7	1.04	
		8.48	4500	600	59.8	51.9	51.9	97.0	2.49	1.22	0.64	55.6	0.93	158.3	1.63	0.71	1.22	0.64	55.6	0.93	
		8.48	4500	750	62.9	51.9	51.9	97.0	2.78	1.22	0.64	60.7	0.86	158.3	1.63	0.71	1.22	0.64	60.7	0.86	
		8.48	6000	150	27.9	30.1	27.9	65.5	1.51	1.22	0.64	25.5	1.10	89.1	1.36	1.10	1.61	0.75	25.4	1.10	
U2_L5	100x40x2.0	8.48	6000	300	35.2	33.6	33.6	65.5	2.14	1.22	0.64	33.4	1.01	89.1	1.36	1.10	1.61	0.75	29.0	1.16	
		8.48	6000	450	38.6	33.6	33.6	65.5	2.62	1.22	0.64	39.1	0.86	89.1	1.36	1.10	1.61	0.75	31.4	1.07	
		8.48	6000	600	39.8	33.6	33.6	65.5	3.03	1.22	0.64	43.8	0.77	89.1	1.36	1.10	1.61	0.75	33.2	1.01	
		8.48	6000	750	40.3	33.6	33.6	65.5	3.38	1.22	0.64	47.8	0.70	89.1	1.36	1.10	1.61	0.75	34.7	0.97	
U2_L6	100x40x2.0	8.48	7000	150	24.2	23.5	23.5	54.5	1.66	1.22	0.64	22.8	1.03	65.5	1.20	1.36	1.87	0.83	21.3	1.10	
		8.48	7000	300	29.1	25.6	25.6	54.5	2.35	1.22	0.64	29.8	0.86	65.5							

Column	Geometry			SFEA				DSM Design												
	$b_w \times b_f \times t$	$\beta_{FT}$	$L$	$f_y$	$P_{u,FT}$	$P_{u,Fm}$	$P_u$	$f_{crFT}$	$\lambda_{FT}$	$b$	$a$	$P_{nFT}$	$\frac{P_u}{P_{nFT}}$	$f_{crFm}$	$R_G$	$c$	$b$	$a$	$P_{nFT-G}$	$\frac{P_u}{P_{nFT-G}}$
U3_L6	100x60x2.0	8.48	8000	150	24.2	18.7	18.7	47.2	1.78	1.22	0.64	20.9	0.90	50.1	1.06	1.72	2.00	0.88	18.2	1.03
		8.48	8000	300	24.2	20.1	20.1	47.2	2.52	1.22	0.64	27.3	0.73	50.1	1.06	1.72	2.00	0.88	18.2	1.10
		8.48	8000	450	24.2	20.1	20.1	47.2	3.09	1.22	0.64	32.0	0.63	50.1	1.06	1.72	2.00	0.88	18.2	1.10
		8.48	8000	600	24.2	20.1	20.1	47.2	3.57	1.22	0.64	35.8	0.56	50.1	1.06	1.72	2.00	0.88	18.2	1.10
		8.48	8000	750	24.2	20.1	20.1	47.2	3.99	1.22	0.64	39.1	0.51	50.1	1.06	1.72	2.00	0.88	18.2	1.10
U4_L1	100x60x3.0	7.15	3300	150	80.5	81.8	80.5	190.3	0.89	1.14	0.62	71.2	1.13	294.4	1.55	0.71	1.14	0.62	71.2	1.13
		7.15	3300	300	112.2	134.6	112.2	190.3	1.26	1.14	0.62	102.4	1.10	294.4	1.55	0.71	1.14	0.62	102.4	1.10
		7.15	3300	450	126.1	158.4	126.1	190.3	1.54	1.14	0.62	112.6	1.12	294.4	1.55	0.71	1.14	0.62	112.6	1.12
		7.15	3300	600	137.9	162.4	137.9	190.3	1.78	1.14	0.62	127.4	1.08	294.4	1.55	0.71	1.14	0.62	127.4	1.08
		7.15	3300	750	149.2	162.4	149.2	190.3	1.99	1.14	0.62	140.3	1.06	294.4	1.55	0.71	1.14	0.62	140.3	1.06
U4_L2	100x60x3.0	7.15	3700	150	75.9	77.2	75.9	163.0	0.96	1.14	0.62	67.4	1.13	234.3	1.44	0.90	1.32	0.67	67.4	1.13
		7.15	3700	300	100.3	116.8	100.3	163.0	1.36	1.14	0.62	91.6	1.09	234.3	1.44	0.90	1.32	0.67	91.6	1.09
		7.15	3700	450	112.9	132.0	112.9	163.0	1.66	1.14	0.62	103.1	1.09	234.3	1.44	0.90	1.32	0.67	101.2	1.12
		7.15	3700	600	124.1	136.0	124.1	163.0	1.92	1.14	0.62	116.7	1.06	234.3	1.44	0.90	1.32	0.67	111.5	1.11
		7.15	3700	750	132.7	136.0	132.7	163.0	2.15	1.14	0.62	128.4	1.03	234.3	1.44	0.90	1.32	0.67	120.2	1.10
U4_L3	100x60x3.0	7.15	4100	150	71.3	71.9	71.3	143.0	1.02	1.14	0.62	63.8	1.12	190.9	1.33	1.15	1.58	0.74	63.8	1.12
		7.15	4100	300	91.1	101.0	91.1	143.0	1.45	1.14	0.62	82.3	1.11	190.9	1.33	1.15	1.58	0.74	82.3	1.11
		7.15	4100	450	102.3	110.9	102.3	143.0	1.77	1.14	0.62	95.7	1.07	190.9	1.33	1.15	1.58	0.74	88.8	1.15
		7.15	4100	600	111.5	113.5	111.5	143.0	2.05	1.14	0.62	108.3	1.03	190.9	1.33	1.15	1.58	0.74	94.3	1.18
		7.15	4100	750	118.1	113.5	113.5	143.0	2.29	1.14	0.62	119.2	0.95	190.9	1.33	1.15	1.58	0.74	98.9	1.15
U4_L4	100x60x3.0	7.15	4600	150	65.9	64.2	64.2	124.8	1.10	1.14	0.62	59.9	1.07	151.7	1.22	1.34	1.77	0.80	59.9	1.07
		7.15	4600	300	81.8	83.8	81.8	124.8	1.55	1.14	0.62	74.4	1.10	151.7	1.22	1.34	1.77	0.80	72.8	1.12
		7.15	4600	450	91.1	89.8	89.8	124.8	1.90	1.14	0.62	88.5	1.01	151.7	1.22	1.34	1.77	0.80	76.3	1.18
		7.15	4600	600	97.7	92.4	92.4	124.8	2.19	1.14	0.62	100.2	0.92	151.7	1.22	1.34	1.77	0.80	78.8	1.17
		7.15	4600	750	101.0	92.4	92.4	124.8	2.45	1.14	0.62	110.3	0.84	151.7	1.22	1.34	1.77	0.80	80.9	1.14
U4_L5	100x60x3.0	7.15	5000	150	62.0	58.3	58.3	113.8	1.15	1.14	0.62	57.0	1.02	128.4	1.13	1.51	1.94	0.86	57.0	1.02
		7.15	5000	300	75.2	72.6	72.6	113.8	1.62	1.14	0.62	70.6	1.03	128.4	1.13	1.51	1.94	0.86	66.2	1.10
		7.15	5000	450	83.2	77.2	77.2	113.8	1.99	1.14	0.62	84.0	0.92	128.4	1.13	1.51	1.94	0.86	67.0	1.15
		7.15	5000	600	87.8	78.5	78.5	113.8	2.30	1.14	0.62	95.1	0.83	128.4	1.13	1.51	1.94	0.86	67.5	1.16
		7.15	5000	750	89.8	78.5	78.5	113.8	2.57	1.14	0.62	104.7	0.75	128.4	1.13	1.51	1.94	0.86	67.9	1.16
U4_L6	100x60x3.0	7.15	5300	150	59.5	54.1	54.1	107.0	1.18	1.14	0.62	55.1	0.98	114.3	1.07	1.70	2.00	0.88	55.1	0.98
		7.15	5300	300	71.3	65.7	65.7	107.0	1.67	1.14	0.62	68.1	0.96	114.3	1.07	1.70	2.00	0.88	62.0	1.06
		7.15	5300	450	77.2	69.3	69.3	107.0	2.05	1.14	0.62	81.1	0.85	114.3	1.07	1.70	2.00	0.88	62.0	1.12
		7.15	5300	600	80.5	70.6	70.6	107.0	2.37	1.14	0.62	91.8	0.77	114.3	1.07	1.70	2.00	0.88	62.0	1.14
		7.15	5300	750	81.2	70.6	70.6	107.0	2.65	1.14	0.62	101.1	0.70	114.3	1.07	1.70	2.00	0.88	62.0	1.14
U4_L7	100x60x3.0	7.15	5600	150	57.0	50.1	50.1	101.3	1.22	1.14	0.62	53.3	0.94	102.3	1.01	1.95	2.00	0.88	53.3	0.94
		7.15	5600	300	67.3	59.5	59.5	101.3	1.72	1.14	0.62	66.0	0.90	102.3	1.01	1.95	2.00	0.88	58.7	1.01
		7.15	5600	450	71.9	59.7	59.7	101.3	2.11	1.14	0.62	78.6	0.76	102.3	1.01	1.95	2.00	0.88	58.7	1.02
		7.15	5600	600	73.9	63.6	63.6	101.3	2.43	1.14	0.62	89.0	0.71	102.3	1.01	1.95	2.00	0.88	58.7	1.08
		7.15	5600	750	74.6	63.6	63.6	101.3	2.72	1.14	0.62	98.0	0.65	102.3	1.01	1.95	2.00	0.88	58.7	1.08
U5_L1	100x80x4.0	4.33	5000	150	104.0	123.8	104.0	125.4	1.09	0.97	0.58	94.6	1.10	234.6	1.87	0.71	0.97	0.58	94.6	1.10
		4.33	5000	300	130.0	187.2	130.0	125.4	1.55	0.97	0.58	118.1	1.10	234.6	1.87	0.71	0.97	0.58	118.1	1.10
		4.33	5000	450	150.8	210.1	150.8	125.4	1.89	0.97	0.58	145.5	1.04	234.6	1.87	0.71	0.97	0.58	145.5	1.04
		4.33	5000	600	168.5	217.4	168.5	125.4	2.19	0.97	0.58	168.8	1.00	234.6	1.87	0.71	0.97	0.58	168.8	1.00
		4.33	5000	750	183.0	217.4	183.0	125.4	2.45	0.97	0.58	189.3	0.97	234.6	1.87	0.71	0.97	0.58	189.3	0.97
U5_L2	100x80x4.0	4.33	6500	150	86.5	97.8	86.5	96.5	1.25	0.97	0.58	81.4	1.06	138.8	1.44	0.89	1.15	0.62	81.4	1.06
		4.33	6500	300	105.0	123.8	105.0	96.5	1.76	0.97	0.58	104.0	1.01	138.8	1.44	0.89	1.15	0.62	101.0	1.04
		4.33	6500	450	117.5	132.1	117.5	96.5	2.16	0.97	0.58	128.2	0.92	138.8	1.44	0.89	1.15	0.62	120.0	0.98
		4.33	6500	600	126.9	135.2	126.9	96.5	2.49	0.97	0.58	148.7	0.85	138.8	1.44	0.89	1.15	0.62	135.5	0.94
		4.33	6500	750	132.1	135.2	132.1	96.5	2.79	0.97	0.58	166.7	0.79	138.8	1.44	0.89	1.15	0.62	149.0	0.89
U5_L3	100x80x4.0	4.33	7000	150	82.0	89.2	82.0	89.1	1.30	0.97	0.58	77.1	1.06	119.7	1.34	1.14	1.40	0.69	77.1	1.06
		4.34	7000	300	98.0	109.2	98.0	89.1	1.83	0.97	0.58	100.1	0.98	119.7	1.34	1.14	1.40	0.69	91.8	1.07
		4.34	7000	450	108.2	114.4	108.2	89.1	2.25	0.97	0.58	123.3	0.88	119.7	1.34	1.14	1.40	0.69	103.8	1.04
		4.34	7000	600	114.4	117.5	114.4	89.1	2.59	0.97	0.58	143.0	0.80	119.7	1.34	1.14	1.40	0.69	113.2	1.01
		4.34	7000	750	118.6	117.5	117.5	89.1	2.90	0.97	0.58	160.4	0.73	119.7	1.34	1.14	1.40	0.69	121.0	0.97
U5_L4	100x80x4.0	4.34	7500	150	77.8	81.1	77.8	83.6	1.34	0.97	0.58	73.6	1.06	104.3	1.25	1.29	1.55	0.73	73.6	1.06
		4.34	7500	300	91.6	96.2	91.6	83.6	1.89	0.97	0.58	97.0	0.94	104.3	1.25	1.29	1.55	0.73	84.7	1.08
		4.34	7500	450	99.6	100.7	99.6	83.6	2.32	0.97	0.58	119.5	0.83	104.3	1.25	1.29	1.55	0.73	92.7	1.07
		4.35	7500	600	103.9	102.5	10													

	Geometry			SFEA				DSM Design												
Column	$b_w \times b_f \times t$	$\beta_{FT}$	$L$	$f_y$	$P_{u,FT}$	$P_{u,Fm}$	$P_u$	$f_{cr,FT}$	$\lambda_{FT}$	$b$	$a$	$P_{n,FT}$	$\frac{P_u}{P_{n,FT}}$	$f_{cr,Fm}$	$R_G$	$c$	$b$	$a$	$P_{n,FT-G}$	$\frac{P_u}{P_{n,FT-G}}$
U5_L7	100x80x4.0	4.36	9000	150	67.1	61.2	61.2	71.0	1.45	0.97	0.58	64.4	0.95	72.4	1.02	1.90	2.00	0.88	64.4	0.95
		4.36	9000	300	74.5	68.7	68.7	71.0	2.06	0.97	0.58	89.6	0.77	72.4	1.02	1.90	2.00	0.88	64.8	1.06
		4.36	9000	450	76.9	71.0	71.0	71.0	2.52	0.97	0.58	110.3	0.64	72.4	1.02	1.90	2.00	0.88	64.8	1.10
		4.36	9000	600	77.3	72.1	72.1	71.0	2.91	0.97	0.58	127.9	0.56	72.4	1.02	1.90	2.00	0.88	64.8	1.11
		4.37	9000	750	77.3	72.2	72.2	71.0	3.25	0.97	0.58	143.5	0.50	72.4	1.02	1.90	2.00	0.88	64.8	1.11
U6_L1	100x80x5.0	3.99	4900	150	149.5	154.7	149.5	158.5	0.97	0.95	0.57	131.2	1.14	244.4	1.54	0.71	0.95	0.57	131.2	1.14
		3.99	4900	300	192.4	234.0	192.4	158.5	1.38	0.95	0.57	176.6	1.09	244.4	1.54	0.71	0.95	0.57	176.6	1.09
		3.99	4900	450	214.5	258.7	214.5	158.5	1.68	0.95	0.57	204.3	1.05	244.4	1.54	0.71	0.95	0.57	204.3	1.05
		3.99	4900	600	232.7	262.6	232.7	158.5	1.95	0.95	0.57	237.6	0.98	244.4	1.54	0.71	0.95	0.57	237.6	0.98
		3.99	4900	750	249.6	262.6	249.6	158.5	2.18	0.95	0.57	267.2	0.93	244.4	1.54	0.71	0.95	0.57	267.2	0.93
U6_L2	100x80x5.0	3.99	5300	150	144.3	148.2	144.3	146.8	1.01	0.95	0.57	127.1	1.13	208.9	1.42	0.94	1.18	0.63	127.1	1.13
		3.99	5300	300	180.7	214.5	180.7	146.8	1.43	0.95	0.57	165.8	1.09	208.9	1.42	0.94	1.18	0.63	165.8	1.09
		3.99	5300	450	200.2	237.9	200.2	146.8	1.75	0.95	0.57	197.0	1.02	208.9	1.42	0.94	1.18	0.63	190.1	1.05
		3.99	5300	600	215.8	248.3	215.8	146.8	2.02	0.95	0.57	229.1	0.94	208.9	1.42	0.94	1.18	0.63	213.8	1.01
		3.99	5300	750	228.8	253.5	228.8	146.8	2.26	0.95	0.57	257.6	0.89	208.9	1.42	0.94	1.18	0.63	234.3	0.98
U6_L3	100x80x5.0	3.99	5700	150	137.8	140.4	137.8	137.1	1.05	0.95	0.57	123.4	1.12	180.6	1.32	1.18	1.42	0.69	123.4	1.12
		3.99	5700	300	170.3	192.4	170.3	137.1	1.48	0.95	0.57	156.1	1.09	180.6	1.32	1.18	1.42	0.69	156.1	1.09
		3.99	5700	450	187.2	209.3	187.2	137.1	1.81	0.95	0.57	190.7	0.98	180.6	1.32	1.18	1.42	0.69	174.4	1.07
		3.99	5700	600	200.2	217.1	200.2	137.1	2.09	0.95	0.57	221.8	0.90	180.6	1.32	1.18	1.42	0.69	189.5	1.06
		3.99	5700	750	210.6	221.0	210.6	137.1	2.34	0.95	0.57	249.4	0.84	180.6	1.32	1.18	1.42	0.69	202.1	1.04
U6_L4	100x80x5.0	3.99	6100	150	132.6	131.3	131.3	128.9	1.08	0.95	0.57	119.8	1.10	157.7	1.22	1.33	1.57	0.74	119.8	1.10
		3.99	6100	300	161.2	172.9	161.2	128.9	1.53	0.95	0.57	149.7	1.08	157.7	1.22	1.33	1.57	0.74	148.1	1.09
		3.99	6100	450	175.5	184.6	175.5	128.9	1.87	0.95	0.57	185.2	0.95	157.7	1.22	1.33	1.57	0.74	161.6	1.09
		3.99	6100	600	185.9	191.1	185.9	128.9	2.16	0.95	0.57	215.4	0.86	157.7	1.22	1.33	1.57	0.74	172.0	1.08
		3.99	6100	750	192.4	193.7	192.4	128.9	2.41	0.95	0.57	242.2	0.79	157.7	1.22	1.33	1.57	0.74	180.4	1.07
U6_L5	100x80x5.0	3.99	6600	150	126.8	120.1	120.1	120.0	1.12	0.95	0.57	115.6	1.04	134.7	1.12	1.53	1.77	0.80	115.6	1.04
		3.99	6600	300	149.5	150.8	149.5	120.0	1.58	0.95	0.57	144.7	1.03	134.7	1.12	1.53	1.77	0.80	138.6	1.08
		3.99	6600	450	161.2	159.9	159.9	120.0	1.94	0.95	0.57	179.0	0.89	134.7	1.12	1.53	1.77	0.80	145.2	1.10
		3.99	6600	600	167.7	163.8	163.8	120.0	2.24	0.95	0.57	208.2	0.79	134.7	1.12	1.53	1.77	0.80	150.1	1.09
		3.99	6600	750	171.6	166.4	166.4	120.0	2.50	0.95	0.57	234.1	0.71	134.7	1.12	1.53	1.77	0.80	154.1	1.08
U6_L6	100x80x5.0	3.99	6900	150	123.1	113.6	113.6	115.3	1.14	0.95	0.57	113.1	1.00	123.3	1.07	1.69	1.93	0.85	113.1	1.00
		3.99	6900	300	144.3	139.1	139.1	115.3	1.61	0.95	0.57	142.0	0.98	123.3	1.07	1.69	1.93	0.85	132.2	1.05
		3.99	6900	450	153.4	146.9	146.9	115.3	1.98	0.95	0.57	175.7	0.84	123.3	1.07	1.69	1.93	0.85	134.1	1.10
		3.99	6900	600	158.6	150.8	150.8	115.3	2.28	0.95	0.57	204.3	0.74	123.3	1.07	1.69	1.93	0.85	135.4	1.11
		3.99	6900	750	161.2	153.4	153.4	115.3	2.55	0.95	0.57	229.7	0.67	123.3	1.07	1.69	1.93	0.85	136.4	1.12
U6_L7	100x80x5.0	3.99	7300	150	118.4	105.4	105.4	109.6	1.17	0.95	0.57	110.0	0.96	110.1	1.00	1.98	2.00	0.88	110.0	0.96
		3.99	7300	300	136.5	126.2	126.2	109.6	1.65	0.95	0.57	138.6	0.91	110.1	1.00	1.98	2.00	0.88	125.0	1.01
		3.99	7300	450	143.0	132.6	132.6	109.6	2.03	0.95	0.57	171.5	0.77	110.1	1.00	1.98	2.00	0.88	125.0	1.06
		3.99	7300	600	145.6	135.2	135.2	109.6	2.34	0.95	0.57	199.5	0.68	110.1	1.00	1.98	2.00	0.88	125.0	1.08
		3.99	7300	750	146.9	136.5	136.5	109.6	2.62	0.95	0.57	224.3	0.61	110.1	1.00	1.98	2.00	0.88	125.0	1.09
U7_L1	80x80x5.0	2.71	6500	150	103.1	114.5	103.1	100.7	1.22	0.87	0.56	96.5	1.07	139.7	1.39	1.04	1.20	0.64	96.5	1.07
		2.71	6500	300	121.2	144.0	121.2	100.7	1.73	0.87	0.56	124.2	0.98	139.7	1.39	1.04	1.20	0.64	118.6	1.02
		2.71	6500	450	132.0	153.6	132.0	100.7	2.11	0.87	0.56	156.1	0.85	139.7	1.39	1.04	1.20	0.64	139.4	0.95
		2.71	6500	600	139.2	157.2	139.2	100.7	2.44	0.87	0.56	183.6	0.76	139.7	1.39	1.04	1.20	0.64	156.3	0.89
		2.72	6500	750	145.2	159.6	145.2	100.7	2.73	0.87	0.56	208.2	0.70	139.7	1.39	1.04	1.20	0.64	170.8	0.85
U7_L2	80x80x5.0	2.72	7000	150	97.3	104.4	97.3	94.0	1.26	0.87	0.56	92.3	1.05	120.5	1.28	1.24	1.40	0.69	92.3	1.05
		2.72	7000	300	112.2	127.2	112.2	94.0	1.79	0.87	0.56	120.5	0.93	120.5	1.28	1.24	1.40	0.69	109.9	1.02
		2.72	7000	450	121.2	133.2	121.2	94.0	2.19	0.87	0.56	151.5	0.80	120.5	1.28	1.24	1.40	0.69	124.0	0.98
		2.72	7000	600	127.2	136.8	127.2	94.0	2.53	0.87	0.56	178.1	0.71	120.5	1.28	1.24	1.40	0.69	135.1	0.94
		2.72	7000	750	130.8	138.0	130.8	94.0	2.82	0.87	0.56	202.0	0.65	120.5	1.28	1.24	1.40	0.69	144.3	0.91
U7_L3	80x80x5.0	2.72	7500	150	91.8	94.9	91.8	87.8	1.31	0.87	0.56	88.0	1.04	104.9	1.19	1.38	1.54	0.73	88.0	1.04
		2.72	7500	300	104.2	112.2	104.2	87.8	1.85	0.87	0.56	117.0	0.89	104.9	1.19	1.38	1.54	0.73	101.8	1.02
		2.72	7500	450	110.8	117.2	110.8	87.8	2.26	0.87	0.56	147.0	0.75	104.9	1.19	1.38	1.54	0.73	111.7	0.99
		2.72	7500	600	115.0	119.6	115.0	87.8	2.61	0.87	0.56	172.9	0.67	104.9	1.19	1.38	1.54	0.73	119.3	0.96
		2.73	7500	750	117.6	121.2	117.6	87.8	2.92	0.87	0.56	196.0	0.60	104.9	1.19	1.38	1.54	0.73	125.6	0.94
U7_L4	80x80x5.0	2.73	8000	150	86.6	86.3	86.3	82.1	1.35	0.87	0.56	83.8	1.03	92.2	1.12	1.53	1.69	0.77	83.8	1.03
		2.73	8000	300	96.8	99.7	96.8	82.1	1.91	0.87	0.56	113.6	0.85	92.2	1.12	1.53	1.69	0.77	93.2	1.04
		2.73	8000	450	101.6	103.7	101.6	82.1	2.34	0.87	0.56	142.7	0.71							

Column	Geometry			SFEA				DSM Design												
	$b_w \times b_f \times t$	$\beta_{FT}$	$L$	$f_y$	$P_{u,FT}$	$P_{u,Fm}$	$P_u$	$f_{crFT}$	$\lambda_{FT}$	$b$	$a$	$P_{nFT}$	$\frac{P_u}{P_{nFT}}$	$f_{crFm}$	$R_G$	$c$	$b$	$a$	$P_{nFT-G}$	$\frac{P_u}{P_{nFT-G}}$
U8_L1	90x90x6.0	2.65	7000	150	150.7	162.0	150.7	112.7	1.15	0.87	0.55	139.2	1.08	152.5	1.35	1.12	1.28	0.65	139.2	1.08
		2.65	7000	300	178.2	210.6	178.2	112.7	1.63	0.87	0.55	176.2	1.01	152.5	1.35	1.12	1.28	0.65	170.3	1.05
		2.65	7000	450	192.8	225.2	192.8	112.7	2.00	0.87	0.55	221.6	0.87	152.5	1.35	1.12	1.28	0.65	197.1	0.98
		2.65	7000	600	204.1	231.7	204.1	112.7	2.31	0.87	0.55	260.7	0.78	152.5	1.35	1.12	1.28	0.65	218.8	0.93
U8_L2	90x90x6.0	2.66	7500	150	143.2	149.9	143.2	105.4	1.19	0.87	0.55	133.9	1.07	132.8	1.26	1.27	1.43	0.70	133.9	1.07
		2.66	7500	300	165.2	186.3	165.2	105.4	1.69	0.87	0.55	171.1	0.97	132.8	1.26	1.27	1.43	0.70	160.1	1.03
		2.66	7500	450	178.2	197.6	178.2	105.4	2.07	0.87	0.55	215.2	0.83	132.8	1.26	1.27	1.43	0.70	179.6	0.99
		2.66	7500	600	186.3	202.5	186.3	105.4	2.39	0.87	0.55	253.2	0.74	132.8	1.26	1.27	1.43	0.70	194.9	0.96
U8_L3	90x90x6.0	2.66	8000	150	135.9	138.0	135.9	98.8	1.23	0.87	0.55	128.7	1.06	116.7	1.18	1.40	1.56	0.73	128.7	1.06
		2.66	8000	300	155.4	166.9	155.4	98.8	1.74	0.87	0.55	166.4	0.93	116.7	1.18	1.40	1.56	0.73	150.0	1.04
		2.66	8000	450	165.2	175.0	165.2	98.8	2.13	0.87	0.55	209.2	0.79	116.7	1.18	1.40	1.56	0.73	164.0	1.01
		2.66	8000	600	171.7	178.2	171.7	98.8	2.46	0.87	0.55	246.2	0.70	116.7	1.18	1.40	1.56	0.73	174.7	0.98
U8_L4	90x90x6.0	2.66	8500	150	129.0	126.8	126.8	92.7	1.27	0.87	0.55	123.4	1.03	103.4	1.12	1.55	1.71	0.78	123.4	1.03
		2.66	8500	300	145.3	149.4	145.3	92.7	1.80	0.87	0.55	161.8	0.90	103.4	1.12	1.55	1.71	0.78	139.0	1.05
		2.66	8500	450	152.6	156.2	152.6	92.7	2.20	0.87	0.55	203.5	0.75	103.4	1.12	1.55	1.71	0.78	147.5	1.03
		2.66	8500	600	157.0	159.2	157.0	92.7	2.54	0.87	0.55	239.4	0.66	103.4	1.12	1.55	1.71	0.78	153.8	1.02
U8_L5	90x90x6.0	2.66	9000	150	122.3	116.5	116.5	87.2	1.31	0.87	0.55	118.3	0.98	92.2	1.06	1.74	1.90	0.84	118.3	0.98
		2.66	9000	300	135.9	134.5	134.5	87.2	1.85	0.87	0.55	157.6	0.85	92.2	1.06	1.74	1.90	0.84	126.7	1.06
		2.66	9000	450	141.3	140.0	140.0	87.2	2.27	0.87	0.55	198.2	0.71	92.2	1.06	1.74	1.90	0.84	129.4	1.08
		2.66	9000	600	144.2	142.6	142.6	87.2	2.62	0.87	0.55	233.1	0.61	92.2	1.06	1.74	1.90	0.84	131.4	1.09
U8_L6	90x90x6.0	2.66	9500	150	116.0	107.1	107.1	82.1	1.35	0.87	0.55	113.1	0.95	82.8	1.01	1.96	2.00	0.88	113.1	0.95
		2.66	9500	300	127.2	121.8	121.8	82.1	1.91	0.87	0.55	153.5	0.79	82.8	1.01	1.96	2.00	0.88	116.7	1.04
		2.66	9500	450	130.9	126.2	126.2	82.1	2.34	0.87	0.55	193.0	0.65	82.8	1.01	1.96	2.00	0.88	116.7	1.08
		2.66	9500	600	132.5	128.5	128.5	82.1	2.70	0.87	0.55	227.1	0.57	82.8	1.01	1.96	2.00	0.88	116.7	1.10
		2.67	9500	750	133.2	129.8	129.8	82.1	3.02	0.87	0.55	257.6	0.50	82.8	1.01	1.96	2.00	0.88	116.7	1.11
												Mean	0.865						Mean	1.039
												Sd.Dev.	0.165						Sd.Dev.	0.076
												Max	1.139						Max	1.182
												Min	0.472						Min	0.850